Journal of Nuclear Medicine, published on November 9, 2018 as doi:10.2967/jnumed.118.218495

Discovery of ^{18}F-JK-PSMA-7, a novel PET-probe for the detection of small PSMA positive lesions

Boris D. Zlatopolskiy[1,2,3]*, Heike Endepols[1,2,4,]*, Philipp Krapf[1,2], Mehrab Guliyev[1], Elizaveta A. Urusova[1,2], Raphael Richarz[1,2], Melanie Hohberg[4], Markus Dietlein[4], Alexander Drzezga[4], Bernd Neumaier[1,2,3]

[1] Institute of Radiochemistry and Experimental Molecular Imaging (IREMB), University Hospital of Cologne, 50937 Cologne; Germany

[2] Institute of Neuroscience and Medicine, INM-5: Nuclear Chemistry, Forschungszentrum Jülich GmbH, 52425 Jülich; Germany

[3] Max Planck Institute for Metabolism Research, 50931 Cologne; Germany

[4] Department of Nuclear Medicine, University Hospital of Cologne, 50937 Cologne, Germany

* Equal contribution of first authors.

Corresponding author:

Prof. Dr. Bernd Neumaier Institute of Neuroscience and Medicine, INM-5: Nuclear Chemistry, Forschungszentrum Jülich GmbH, Wilhelm-Johnen-Straße, 52425 Jülich, Germany, phone: +49-2461-61-4141, fax: +49-2461-61-2535, b.neumaier@fz-juelich.de

First author:

Priv.-Doz. Dr. Boris Zlatopolskiy, Institute of Radiochemistry and Experimental Molecular Imaging (IREMB), University Hospital of Cologne, Kerpener Str. 62, 50937 Cologne, Germany. Phone: +49-221-478 82842, fax: +49-221-47882844, boris.zlatopolskiy@uk-koeln.de

Word count: 4993

Running title: ^{18}F-JK-PSMA-7 for PSMA positive lesions

ABSTRACT

Prostate specific membrane antigen (PSMA) expressed by the vast majority of prostate cancers (PCa) is a promising target for PCa imaging. The application of PSMA specific ^{18}F-labeled PET probes like ^{18}F-DCFPyL and ^{18}F-PSMA-1007 considerably improved the accuracy of PCa tumor detection. However, there remains a need for further improvements regarding sensitivity and specificity. The aim of this study was the development of highly selective and specific PSMA probes with enhanced imaging properties, in comparison with ^{18}F-DCFPyL, ^{18}F-PSMA-1007 and ^{68}Ga-PSMA-11. **Methods:** Eight novel ^{18}F-labeled PSMA ligands were prepared. Their cellular uptake in PSMA$^+$ LNCaP C4-2 and PSMA$^-$ PC-3 cells was compared to that of ^{18}F-DCFPyL. The most promising candidates were additionally evaluated by µPET in healthy rats using PSMA$^+$ peripheral ganglia as a model for small PCa lesions. PET images of the ligand with the best outcome, ^{18}F-JK-PSMA-7, were compared to those of ^{18}F-DCFPyL, ^{18}F-PSMA-1007 and ^{68}Ga-PSMA-11 with respect to key image quality parameters for the time frame 60-120 min. **Results:** Compared to ^{18}F-DCFPyL, ^{18}F-JK-PSMA-7 demonstrated increased PSMA specific cellular uptake. While target-to-background ratios of ^{18}F-DCFPyL and ^{18}F-PSMA-1007 were comparable, this parameter was higher for ^{18}F-JK-PSMA-7 and lower for ^{68}Ga-PSMA-11. Image acutance was significantly higher for ^{18}F-JK-PSMA-7 and ^{18}F-PSMA-1007 compared to ^{18}F-DCFPyL and ^{68}Ga-PSMA-11. Image resolution was similar for all four tracers. ^{18}F-PSMA-1007 demonstrated significantly higher blood protein binding and bone uptake than the other tracers. **Conclusion:** ^{18}F-JK-PSMA-7 is a promising candidate for high quality visualization of small PSMA-positive lesions. Excellent preclinical imaging properties justify further preclinical and clinical studies of this tracer.

Keywords: Prostate carcinoma; PSMA; radiofluorination; positron emission tomography; imaging; preclinical model

INTRODUCTION

Prostate-specific membrane antigen (PSMA) is expressed by the vast majority of prostate carcinomas (PCas). The level of PSMA expression correlates with tumor aggressiveness (*1*). Consequently, PSMA represents an excellent molecular target for PCa imaging. ^{68}Ga-PSMA PET is already widely used for PCa diagnostics (*2*). However, the growing demand for PSMA imaging agents stimulated the development of ^{18}F-labeled PSMA ligands. Among them ^{18}F-DCFPyL (*3*) has been already evaluated in several clinical centers (*4-10*). Nevertheless, some limitations remain with respect to pharmacokinetics and detection rates in patients with very low PSA-values (<1 ng/mL). Thus, there is still room for the development of more sensitive PSMA specific probes. Importantly, availability on a preparative scale using efficient cGMP procedures amenable to automation is a prerequisite for its clinical applications. Here we present eight novel radiofluorinated candidates (Fig. 1) together with their *in vitro* and *in vivo* evaluation.

MATERIALS AND METHODS

Preparation of PSMA-Specific PET Probes

^{68}Ga-PSMA-11 and ^{18}F-PSMA-1007 were synthesized according to Eder et al. (*11*) and Cardinale et al. (*12*), respectively. ^{18}F-DCFPyL (^{18}F-**2**), ^{18}F-JK-PSMA-7–9 (^{18}F-**4**–**6**), and ^{18}F-JK-PSMA-11–13 (^{18}F-**8**–**10**) were prepared using the “minimalist” approach (*13*) according to the modified protocol of Neumaier et al. (*14*) (Fig. 2; Supplemental Fig. 1). For the manual synthesis and automated production of ^{18}F-JK-PSMA-7 on a FXNPro module (GE) refer to Supplemental Fig. 2. ^{18}F-JK-PSMA-10 (^{18}F-**7**) was prepared implementing the “minimalist” protocol to the procedure proposed for the preparation of ^{18}F-DCFPyL by Bouvet et al. (*15*) and by Ravert et al. (*16*). ^{18}F-JK-PSMA-14 (^{18}F-**11**) was prepared as described elsewhere (*17*). For the preparation

of intermediates, precursors for radiolabeling and reference compounds refer to Supplemental Data and (*18*-*22*).

Cellular Uptake Studies

Cells were cultivated as described in Supplemental Data. The PET tracer was added to the cells (100–150 kBq/well, 3 wells per tracer) and incubated at 37 °C for 2 and 4 h. 2-(Phosphonomethyl)pentanedioic acid (2-PMPA; 100 µm/well) was used for blocking studies. Cells were trypsinized, harvested and measured in a gamma counter (Wizard 1470, PerkinElmer, Massachusetts, USA), and % uptake per 10^5 cells was calculated. Uptake of ^{18}F-DCFPyL was always measured in parallel. Cellular uptake values were compared using 2-way Analysis of variance (ANOVA) followed by Sidak's multiple comparison test ($p<0.05$).

PET Evaluation of PSMA Specific Tracers in Healthy Rats

Healthy Long Evans rats (11 males, 2 females; 250–530 g) were used for this study. Rats were housed in groups of 2-4 animals under controlled conditions (22±1 °C and 55±5% rh) and an inversed 12-h light/dark schedule (lights on 8:30 p.m–8:30 a.m.). Rats had free access to water and food. Experiments were carried out in accordance with the European Union directive 2010/63/EU for animal experiments, and were approved by regional authorities (Ministry for Environment, North Rhine-Westphalia).

Prior to PET measurements, animals were anesthetized [initially 5% isoflurane in O_2/air (3:7), then reduction to 2%], and a catheter for tracer injection was inserted into the lateral tail vein. Dynamic PET scans in list mode were performed using a Focus 220 micro PET scanner (CTI-Siemens, Germany). Data acquisition started with tracer injection (17–77 MBq in 0.5 mL), continued for 120 min and was followed by a 10 min transmission scan using a ^{57}Co point source. For blocking studies, the PSMA-inhibitor 2-PMPA (23 mg/kg) was injected together with the radiotracer. Body temperature was maintained at 37 °C by a feedback-controlled system.

Images were reconstructed using an iterative OSEM3D/MAP procedure (*23*) resulting in voxel sizes of 0.38×0.38×0.80 mm. The 120 min measurement was divided into different time frames: a) 2×60 min, b) 4×30 min, c) for time-activity curves: 2×1 min, 2×2 min, 6×4 min, 18×5 min. Postprocessing and image analysis was performed with VINCI 4.72 (Max Planck Institute for Metabolism Research, Cologne, Germany). Frames were Gauss-filtered (1 mm full width at half maximum [FWHM]) and intensity-normalized to injected dose, corrected for body weight (SUV_{BW}). Tracer tissue accumulation was measured for the 60–120 min frame and compared between tracers using one-way ANOVA followed by Dunnett's multiple comparisons test.

Analysis of PET Image Quality

Target-to-Background Ratio (TBR). This parameter describes the delineation of PSMA-positive ganglia against PSMA-negative background. Two elliptical volumes of interest (VOIs) were used: The first VOI (150 voxels) was placed over the superior cervical ganglion (SCG) and the second (1600 voxels) over the neck region dorsal from the spinal cord. VOI mean values were extracted and the SCG/background ratio was calculated. TBR was first determined for candidate probes (^{18}F-JK-PSMA-7–11 and -13) and compared with ^{18}F-DCFPyL in the same animal for the time frame 60–120 min. The most promising candidate, ^{18}F-JK-PSMA-7 (56–63 MBq), its regioisomer, ^{18}F-JK-PSMA-8 (47–70 MBq), ^{18}F-DCFPyL (45–71 MBq), ^{18}F-PSMA-1007 (17–59 MBq) and ^{68}Ga-PSMA-11 (13–51 MBq) were evaluated each in three animals. ^{18}F-JK-PSMA-9–11 and -13 were not further evaluated.

Acutance. The image intensity of a PSMA-positive ganglion decreases gradually to background, forming a slope which reflects the edge contrast or acutance. An 8 mm profile (1 pixel width) was placed over the middle of the SCG (diameter approx. 3.5 mm) in the horizontal plane. The slope of the profile plot was determined by dividing the maximum height of the SCG profile (peak minus background) by its FWHM. The time frame used for this analysis was 60–120 min p.i..

Resolution. The dorsal root ganglia (DRG) are arranged in pairs along the spinal cord. The parameter "spatial resolution" describes how well the two ganglia of one pair can be separated from each other. A 12 mm profile was placed over the first cervical pair of DRG (ganglion diameter approx. 2.5 mm; distance from center to center: approx. 4 mm) in the horizontal plane. We employed the formula commonly used in chromatography (*24*):

$$R = \frac{2(P1 - P2)}{1.7(FWHM1 + FWHM2)}$$

with R: resolution; P1-P2: distance between peaks.

Image quality parameters were compared between tracers using one-way ANOVA followed by Dunnett's multiple comparisons test. In addition, TBRs were compared using two-way ANOVA with the factors "tracer" and "frame", followed by Tukey's multiple comparisons test. The time frame analyzed was 60–120 min p.i.

Patient PET/CT Scan

A first-in-man study with ^{18}F-JK-PSMA-7 in a patient was carried out within the clinical workup. The patient had given his written informed consent for PET imaging and the scientific evaluation of his data. All procedures were performed in accordance with the Institutional Review Board and in compliance with the regulations of the responsible local authorities (Bezirksregierung Köln, Cologne, Germany).

RESULTS

Preparation of PET Probes

^{18}F-DCFPyL and the novel PET tracers, ^{18}F-JK-PSMA-7–9 and -11–13 were prepared by the acylation of ureas **24**–**27** with the appropriate ^{18}F-labeled active ester, ^{18}F-**18**–**20**, in anhydrous EtOH using Et_4NHCO_3 as a base and purified by solid phase extraction (SPE) or HPLC (Fig. 2) (*14*). ^{18}F-**18**–**23** were synthesized by direct elution of ^{18}F-fluoride previously

loaded onto an anion exchange resin with a solution of the corresponding radiolabeling precursor in a suitable solvent (EtOH, EtOH/MeCN/*t*BuOH, MeCN/*t*BuOH or MeCN). Subsequently, the solution was heated to 40 °C for 2–5 min (if pure EtOH was used for elution, it was preliminary diluted with a MeCN/*t*BuOH mixture; in this case the reaction time amounted to 15–20 min) and purified by SPE. Using this protocol, ^{18}F-DCFPyL and ^{18}F-JK-PSMA-7–9 and -10–13 were prepared in two steps in n.d.c. RCYs of 12–25%. ^{18}F-**21**–**23** were insufficiently stable and defluorinated rapidly during purification (^{18}F-**22**) or the second reaction step (^{18}F-**21** and ^{18}F-**23**). Consequently, ^{18}F-**7** was prepared starting from **28** using a modified “minimalist” approach (*13*). ^{18}F-Fluoride was eluted from the anion exchange cartridge with a solution of **28** in EtOH and the resulting solution was heated at 150 °C for 20 min affording the protected intermediate which was purified by SPE and deprotected using H_3PO_4 or HCl in aqueous MeCN at 45 °C for 5 min. Finally, ^{18}F-JK-PSMA-10 was isolated by HPLC in 3–5% RCY.

Cellular Uptake Studies

All tested PET-tracers showed a significantly increased uptake in LNCaP cells after 4 h compared to 2 h [$F(1,34)=8081$; $p<0.0001$ for factor "time"; post hoc $p<0.05$]. In contrast, tracer uptake in PSMA$^-$ PC-3 cells was low (Supplemental Fig. 3 and Supplemental Table 1). The PSMA specificity of tracer uptake in LNCaP C4-2 cells was confirmed by the inhibition with 2-PMPA.

Comparison between uptake in LNCaP C4-2 cells of ^{18}F-**4**–**11** in relation to that of ^{18}F-DCFPyL is shown in Fig. 3. Only ^{18}F-JK-PSMA-7 exhibited a significantly higher cellular uptake than ^{18}F-DCFPyL after 2 h [$F(7,38)=1136$; $p<0.0001$ for factor „tracer“, post hoc $p<0.05$]. For all other tracers uptake in LNCaP C4-2 cells after 2 h was significantly lower than that of ^{18}F-DCFPyL (Supplemental Table 2). After 4 h, cellular uptake of ^{18}F-JK-PSMA-7 in LNCaP C4-2 cells was also significantly higher, while uptake of ^{18}F-JK-PSMA-9 and -11 was comparable to

that of ^{18}F-DCFPyL. All other tracers showed a significantly lower uptake after 4 h. Owing to the low PSMA-specific cellular uptake, ^{18}F-JK-PSMA-12 and -14 were excluded from further studies.

Initial *in vivo* Experiments

Stability towards defluorination as well as TBR of the PET tracers were determined in healthy rats using µPET. All tracers except ^{18}F-JK-PSMA-10 were sufficiently stable *in vivo* (Supplemental Fig. 4 and 5). TBR determined for the SCG was highest for ^{18}F-JK-PSMA-7 followed by ^{18}F-DCFPyL, ^{18}F-PSMA-1007, ^{18}F-JK-PSMA-8 and finally ^{68}Ga-PSMA-11 (Fig. 4B, Table 1). Analysis of 4×30 min frames revealed that TBR of ^{18}F-JK-PSMA-7 and ^{18}F-PSMA-1007 increased over time (Fig. 4C). Notably, ^{18}F-PSMA-1007 demonstrated the highest SCG accumulation (94.8±19.6 SUV_{BW}). However, owing to the high background radioactivity of 15.86±1.68 SUV_{BW}, TBR of this tracer was not higher than TBR of ^{18}F-DCFPyL and ^{18}F-JK-PSMA-7. TBR for ^{18}F-JK-PSMA-9 (4.0), ^{18}F-JK-PSMA-10 (2.1), ^{18}F-JK-PSMA-11 (2.6) and ^{18}F-JK-PSMA-13 (4.3) were determined once in the same animal (Supplemental Fig. 4). Owing to their insufficiently high TBR (<4.5) these tracers were not further evaluated.

Biodistribution and Biokinetics of ^{18}F-DCFPyL, ^{18}F-PSMA-1007, ^{18}F-JK-PSMA-7 and -8, and ^{68}Ga-PSMA-11 in Healthy Rats

^{18}F-DCFPyL demonstrated a slow washout in all tissues (Supplemental Fig. 5A, Table 2) comparable with that of ^{18}F-JK-PSMA-7. Liver accumulation of ^{18}F-JK-PSMA-7 reached the maximal value of 302.1±83.2 SUV_{BW} 24 min p.i. (Supplemental Fig. 5B) and decreased to 119.3±8.3 SUV_{BW}. This was still significantly higher compared to ^{18}F-JK-PSMA-8 and ^{18}F-PSMA-1007 [$F(4,10)=7.83$, $p=0.0040$; post hoc $p<0.05$]. Despite the very close structural similarity, biodistribution data of ^{18}F-JK-PSMA-7 and ^{18}F-JK-PSMA-8 revealed significant differences. Bone uptake of ^{18}F-JK-PSMA-8 (19.2±2.1 SUV_{BW}) was 6 times higher than background and twice as high as SCG uptake (Table 2), indicating that defluorination took place (Supplemental Fig. 5C).

Accordingly, tracer uptake in the DRG was completely obscured. Compared to the other tracers, ^{18}F-PSMA-1007 demonstrated a significantly higher accumulation (post hoc $p<0.05$) in all tissues including SCG, salivary gland and bone, but not in the liver (Table 2). The DRG were clearly visible, and the SCG signal reached a plateau with no further washout after 1 h p.i. (Supplemental Fig. 5D). Bone accumulation of ^{18}F-PSMA-1007 was much higher compared to all other tracers, even compared to ^{18}F-JK-PSMA-8. However, tracer biodistribution did not provide evidence for significant defluorination, since bone uptake was almost three times lower than SCG uptake, and only twice as high as background. Uptake of ^{68}Ga-PSMA-11 in evaluated tissues was lower than that of ^{18}F-PSMA-1007 but higher than that of the other tracers (Table 2). Measurement of blood radioactivity in the lumen of the left ventricle revealed a significantly higher value for ^{18}F-PSMA-1007 and for ^{68}Ga-PSMA-11 compared to the other tracers [8.61–16.28 SUV_{BW}; $F(3,8)=53.53$, $p<0.0001$; post hoc $p<0.05$] (Table 2, Supplemental Fig. 6).

Comparison of Image Quality

Acutance measured in the SCG was significantly higher for ^{18}F-JK-PSMA-7 and ^{18}F-PSMA-1007 compared to ^{18}F-DCFPyL and ^{68}Ga-PSMA-11 [$F(4,10)=12.77$, $p=0.0006$, post hoc $p<0.05$; Fig. 5, Table 1]. Spatial resolution, measured for the apical pair of cervical DRG, was significantly higher for ^{18}F-JK-PSMA-7 compared to ^{18}F-JK-PSMA-8 [$F(4,10)=3.80$, $p=0.0396$, post hoc $p<0.05$; Fig. 6, Table 1].

^{18}F-JK-PSMA-7 in a Patient with Prostate Cancer Recurrence

A first-in-man study was conducted with ^{18}F-JK-PSMA-7 (Fig. 7). A 64-y-old patient with an elevated prostate-specific antigen level (130 ng/mL) was referred to PSMA PET/CT before further treatment. A ^{18}F-JK-PSMA-7 PET scan demonstrated tracer accumulation in the prostate, skeletal lesions, and pelvic lymph nodes.

DISCUSSION

^{18}F-DCFPyL, ^{18}F-JK-PSMA-7–9 and -11–13 were prepared using a two-step procedure outlined in Fig. 2. This modular approach enabled the application of the same building blocks for the synthesis of different radiotracers. ^{18}F-Labeled active esters ^{18}F-**18**–**23** were obtained in RCYs of up to 85% within 8–20 min using only ^{18}F-fluoride and the corresponding labeling precursor without any evaporation steps. The acylation step worked well only in anhydrous EtOH. If the reaction was carried out in aprotic or aqueous media, much lower RCCs (0–15%) were observed. The final purification by SPE or HPLC afforded tracers in good RCYs (12–25% n.d.c.) and excellent radiochemical purity (>98%). The simplicity of the preparation procedure enabled a straightforward transfer to synthesis modules. Owing to the insufficient stability of ^{18}F-**20**, ^{18}F-JK-PSMA-13 was prepared from the corresponding protected precursor **28**. The electron-poor nature of the pyridazine ring allowed for the first time high-yielding S_NAr radiofluorination in pure primary alcohols like EtOH in > 90% radiochemical conversions. Unfortunately, it also caused substantial decomposition during the deprotection step.

Next, we started the biological evaluation of the novel radiotracers. Their PSMA-specific cellular uptake was compared to that of ^{18}F-DCFPyL. As the predictive power of *in vitro* stability assays is limited (*25*), the metabolic stability of the candidates was determined in healthy rats. High stability towards *in vivo* defluorination is especially important for PCa imaging. ^{18}F-Fluoride avidly accumulates not only in PCa bone lesions, but also in healthy bones. This could lead to incorrect diagnosis and wrong therapy. PSMA-specific cellular accumulation of ^{18}F-JK-PSMA-9, -11 and ^{18}F-DCFPyL was comparable. In contrast, ^{18}F-JK-PSMA-7 revealed significantly higher accumulation rates. All three ligands were largely inert towards *in vivo* defluorination and were, together with ^{18}F-JK-PSMA-8, the closest structural analog of ^{18}F-JK-PSMA-7, chosen for further studies.

For the *in vivo* evaluation we utilized the rat peripheral ganglia as a model for small focal PSMA-positive lesions making use of their high PSMA expression and small size (2.5–3.5 mm),

comparable, e.g., to the size of small lymph nodes. We determined TBR of the above mentioned candidates in the SCG of rats. Only ^{18}F-JK-PSMA-7 had TBR higher than ^{18}F-DCFPyL. Notably, the small structural difference between JK-PSMA-7 and -8 (methoxy substituent either in 4- or 2-position of the pyridine ring) resulted in different biodistribution. Also, introduction of the 4-ThiaLys (^{18}F-JK-PSMA-10) instead of the Lys residue (^{18}F-DCFPyL) resulted in a lower PSMA-specific cellular uptake *in vitro* and a low TBR *in vivo*.

Subsequently, we evaluated biokinetics and biodistribution of ^{18}F-JK-PSMA-7 and -8, in comparison to ^{18}F-DCFPyL, ^{18}F-PSMA-1007 and ^{68}Ga-PSMA-11 in healthy rats. This study revealed markedly high accumulation of ^{18}F-PSMA-1007 in PSMA-positive ganglia, but also in non-target tissues like neck muscles, blood and bones compared to the other tracers. At the same time, liver uptake of ^{18}F-PSMA-1007 was low, indicating mainly renal elimination. Additionally, this tracer demonstrated significantly slower blood clearance. These differences may be explained by the presence of two acidic Glu residues leading to stronger electrostatic interactions of ^{18}F-PSMA-1007 with Lys- and Arg-rich proteins like serum albumin (*26*). High blood protein binding should delay excretion of the tracer resulting in lower accumulation in kidneys and bladder. This could be advantageous for detecting PCa metastases adjacent to urethra and bladder. On the other hand, higher background radioactivity especially in bone could mask enrichment of the tracer in smaller lesions. While liver uptake of ^{18}F-JK-PSMA-7 was higher compared to ^{18}F-DCFPyL, possibly owing to the presence of the lipophilic methoxy group, liver uptake of the regioisomer ^{18}F-JK-PSMA-8 was significantly lower. We assumed that this apparent discrepancy could be explained by defluorination of ^{18}F-PSMA-8 in the liver, as indicated by radioactivity accumulation in bones.

Image quality has the largest impact on diagnostic accuracy of medical imaging, and TBR is widely used to compare different PET-tracers. In contrast to ^{18}F-DCFPyL, ^{18}F-JK-PSMA-8 and ^{68}Ga-PSMA-11, TBR for ^{18}F-JK-PSMA-7 significantly increased over time. The same effect, although less pronounced, was observed for ^{18}F-PSMA-1007. In order to explain these

differences, we examined TACs of SCG and non-target tissue in more detail. Initially high uptake of ^{18}F-DCFPyL, ^{18}F-JK-PSMA-8 and ^{68}Ga-PSMA-11 in the SCG decreased over time in accordance with the blood input function. This indicates a high amount of unbound tracer (*27*). In contrast, the TACs of ^{18}F-JK-PSMA-7 and ^{18}F-PSMA-1007 decreased more slowly, and intersected the blood input function, finally reaching a plateau above blood radioactivity. This indicates active tracer-target binding and trapping (e.g., by internalization). For ^{18}F-PSMA-1007 and (to a lesser extent) for ^{68}Ga-PSMA-11, however, a significantly longer retention of radioactivity in blood led to increased background activity.

Other important factors, like resolution and acutance (edge contrast) have so far not been used for the qualitative assessment of PET images. High acutance increases the subjective perception of "sharpness" and allows improved measurements of lesion size. Acutance was significantly higher for ^{18}F-JK-PSMA-7 and ^{18}F-PSMA-1007 compared to ^{18}F-DCFPyL, ^{18}F-JK-PSMA-8, and ^{68}Ga-PSMA-11. Resolution is the ability to delineate two small target tissues close to each other. ^{18}F-JK-PSMA-7 exhibited the highest resolution which was slightly lower for ^{18}F-DCFPyL, ^{18}F-PSMA-1007 and ^{68}Ga-PSMA-11. Again, the resolution of ^{18}F-JK-PSMA-7 scans was significantly higher than that of ^{18}F-JK-PSMA-8.

Among the evaluated ligands, ^{18}F-JK-PSMA-7 demonstrated the most favorable properties for imaging of PSMA positive tissues. Owing to the excellent preclinical imaging properties of ^{18}F-JK-PSMA-7, the first observational study on ^{18}F-JK-PSMA-7 PET/CT in patients with biochemical recurrence was initiated. This study suggests promising performance with regard to detection of PSMA-positive tumor tissue. These clinical and dosimetry data were preliminary presented by SNMMI-2018 (*28,29*) and will be published in due course.

CONCLUSIONS

The novel modular production protocol enabled the fast and high-yielding preparation of structurally different PSMA ligands. Application of peripheral ganglia of healthy rats as models of

small PSMA positive lesions allowed fast, precise and cost-effective preclinical screening of PSMA specific PET-ligands. In the direct comparison with the already established PET-tracers, ^{68}Ga-PSMA-11, ^{18}F-DCFPyL and ^{18}F-PSMA-1007, the novel probe, ^{18}F-JK-PSMA-7, in contrast to regioisomeric ^{18}F-JK-PSMA-8, demonstrated favorable properties with respect to image quality and sensitivity to detect small PSMA-positive tissues. Accordingly, careful preclinical and clinical evaluations of ^{18}F-JK-PSMA-7 are under way.

DISCLOSURE

^{18}F-JK-PSMA-7 is the subject of a patent application by B. Zlatopolskiy, P. Krapf, R. Richarz, A. Drzezga and B. Neumaier. There are no any other potential conflicts of interest relevant for this article.

ACKNOWLEDGMENTS

We thank Dr. A. Morgenroth, RWTH Aachen, and Mr. G. Winter, University clinic Ulm, for providing of LNCaP C4-2 cells, Dr. M. Müller, ABX GmbH, Radeberg, for providing of PSMA-1007 and its precursor and Mr. Craig for proofreading of the manuscript.

This study was funded by the LeitmarktAgentur.NRW and the European Regional Development Fund (LS-1-2-023c/EFRE-0800973 and LS-1-2-023b/EFRE-0800992).

REFERENCES

1. Ross JS, Sheehan CE, Fisher HA, et al. Correlation of primary tumor prostate-specific membrane antigen expression with disease recurrence in prostate cancer. *Clin Cancer Res.* 2003;9:6357–6362.

2. Afshar-Oromieh A, Holland-Letz T, Giesel FL, et al. Diagnostic performance of ^{68}Ga-PSMA-11 (HBED-CC) PET/CT in patients with recurrent prostate cancer: evaluation in 1007 patients. *Eur J Nucl Med Mol Imaging.* 2017;44:1258–1268.

3. Chen Y, Pullambhatla M, Foss CA, et al. 2-(3-{1-Carboxy-5-[(6-[^{18}F]fluoro-pyridine-3-carbonyl)-amino]-pentyl}-ureido)-pen tanedioic acid, [^{18}F]DCFPyL, a PSMA-based PET imaging agent for prostate cancer. *Clin Cancer Res.* 2011;17:7645–7653.

4. Szabo Z, Mena E, Rowe SP, et al. Initial evaluation of [^{18}F]DCFPyL for prostate-specific membrane antigen (PSMA)-targeted PET imaging of prostate cancer. *Mol Imaging Biol.* 2015;17:565–574.

5. Rowe SP, Mana-Ay M, Javadi MS, et al. PSMA-based detection of prostate cancer bone lesions with ^{18}F-DCFPyL PET/CT: a sensitive alternative to ^{99m}Tc-MDP bone scan and Na^{18}F PET/CT? *Clin Genitourin Cancer.* 2016;14:e115–118.

6. Rowe SP, Gorin MA, Hammers HJ, Pomper MG, Allaf ME, Javadi MS. Detection of ^{18}F-FDG PET/CT occult lesions with ^{18}F-DCFPyL PET/CT in a patient with metastatic renal cell carcinoma. *Clin Nucl Med.* 2016;41:83–85.

7. Dietlein F, Kobe C, Neubauer S, et al. PSA-stratified performance of ^{18}F- and ^{68}Ga-PSMA PET in patients with biochemical recurrence of prostate cancer. *J Nucl Med.* 2017;58:947–952.

8. Li X, Rowe SP, Leal JP, et al. Semiquantitative parameters in PSMA-targeted PET imaging with ^{18}F-DCFPyL: variability in normal-organ uptake. *J Nucl Med.* 2017;58:942–946.

9. Wondergem M, van der Zant FM, Knol RJJ, Lazarenko SV, Pruim J, de Jong IJ. ^{18}F-DCFPyL PET/CT in the detection of prostate cancer at 60 and 120 minutes: detection rate, image quality, activity kinetics, and biodistribution. *J Nucl Med.* 2017;58:1797–1804.

10. Dietlein M, Kobe C, Kuhnert G, et al. Comparison of [^{18}F]DCFPyL and [^{68}Ga]Ga-PSMA-HBED-CC for PSMA-PET imaging in patients with relapsed prostate cancer. *Mol Imaging Biol.* 2015;17:575–584.

11. Eder M, Neels O, Müller M, et al. Novel preclinical and radiopharmaceutical aspects of [^{68}Ga]Ga-PSMA-HBED-CC: a new pet tracer for imaging of prostate cancer. *Pharmaceuticals (Basel).* 2014;7:779–796.

12. Cardinale J, Martin R, Remde Y, et al. Procedures for the GMP-compliant production and quality control of [^{18}F]PSMA-1007: a next generation radiofluorinated tracer for the detection of prostate cancer. *Pharmaceuticals (Basel).* 2017;10:77.

13. Richarz R, Krapf P, Zarrad F, Urusova EA, Neumaier B, Zlatopolskiy BD. Neither azeotropic drying, nor base nor other additives: a minimalist approach to ^{18}F-labeling. *Org Biomol Chem.* 2014;12:8094–8099.

14. Neumaier B, Zlatopolskiy BD, Richarz R, Krapf P. Method for the production of ^{18}F-labeled active esters and their application exemplified by the preparation of a PSMA-specific PET-tracer. *Patent WO2016030329A1.* 2014.

15. Bouvet V, Wuest M, Jans HS, et al. Automated synthesis of [^{18}F]DCFPyL via direct radiofluorination and validation in preclinical prostate cancer models. *EJNMMI Res.* 2016;6:40.

16. Ravert HT, Holt DP, Chen Y, et al. An improved synthesis of the radiolabeled prostate-specific membrane antigen inhibitor, [^{18}F]DCFPyL. *J Labelled Comp Radiopharm.* 2016;59:439–450.

17. Krapf P, Richarz R, Urusova EA, Neumaier B, Zlatopolskiy BD. Seyferth-gilbert homologation as a route to ^{18}F-labeled building blocks: preparation of radiofluorinated phenylacetylenes and their application in PET chemistry. *European J Org Chem.* 2016;3:430–433.

18. Drennen B, Scheenstra JA, Yap JL, et al. Structural re-engineering of the alpha-helix mimetic JY-1-106 into small molecules: disruption of the Mcl-1-Bak-BH3 protein-protein interaction with 2,6-di-substituted nicotinates. *ChemMedChem.* 2016;11:827–833.

19. Ehara T, Irie O, Kosaka T, et al. Structure-based design of substituted piperidines as a new class of highly efficacious oral direct Renin inhibitors. *ACS Med Chem Lett.* 2014;5:787–792.

20. Gajera JM, Gharat LA, Kattige VG, Khairatkar-Joshi N, Narayana L. Tricyclic compounds as mPGES-1 inhibitors. *Patent WO2012110860A1.* 2011.

21. Kim DW, Jeong HJ, Lim ST, Sohn MH. Tetrabutylammonium tetra(tert-butyl alcohol)-coordinated fluoride as a facile fluoride source. *Angew Chem Int Ed Engl.* 2008;47:8404–8406.

22. Murelli RP, Zhang AX, Michel J, Jorgensen WL, Spiegel DA. Chemical control over immune recognition: a class of antibody-recruiting small molecules that target prostate cancer. *J Am Chem Soc.* 2009;131:17090–17092.

23. Qi J, Leahy RM, Cherry SR, Chatziioannou A, Farquhar TH. High-resolution 3D Bayesian image reconstruction using the microPET small-animal scanner. *Phys Med Biol.* 1998;43:1001–1013.

24. Dolan JW. Peak tailing and resolution. *Lc Gc Europe.* 2002;15:334–337.

25. Zlatopolskiy BD, Zischler J, Schafer D, et al. Discovery of 7-[^{18}F]fluorotryptophan as a novel positron emission tomography (PET) probe for the visualization of tryptophan metabolism in vivo. *J Med Chem.* 2018;61:189–206.

26. Kragh-Hansen U, Chuang VT, Otagiri M. Practical aspects of the ligand-binding and enzymatic properties of human serum albumin. *Biol Pharm Bull.* 2002;25:695–704.

27. Morris ED, Lucas MV, Petrulli JR, Cosgrove KP. How to design PET experiments to study neurochemistry: application to alcoholism. *Yale J Biol Med.* 2014;87:33–54.

28. Hohberg M, Dietlein M, Kobe C, et al. Biodistribution and radiation dosimetry of the novel ^{18}F-labeled prostate-specific membrane antigen-ligand PSMA-7 for PET/CT in prostate cancer patients *J Nucl Med.* 2018;59:88.

29. Dietlein M, Hohberg M, Kobe C, et al. Performance of the novel ^{18}F-labeled prostate-specific membrane antigen-ligand PSMA-7 for PET/CT in prostate cancer patients. *J Nucl Med.* 2018;59:452.

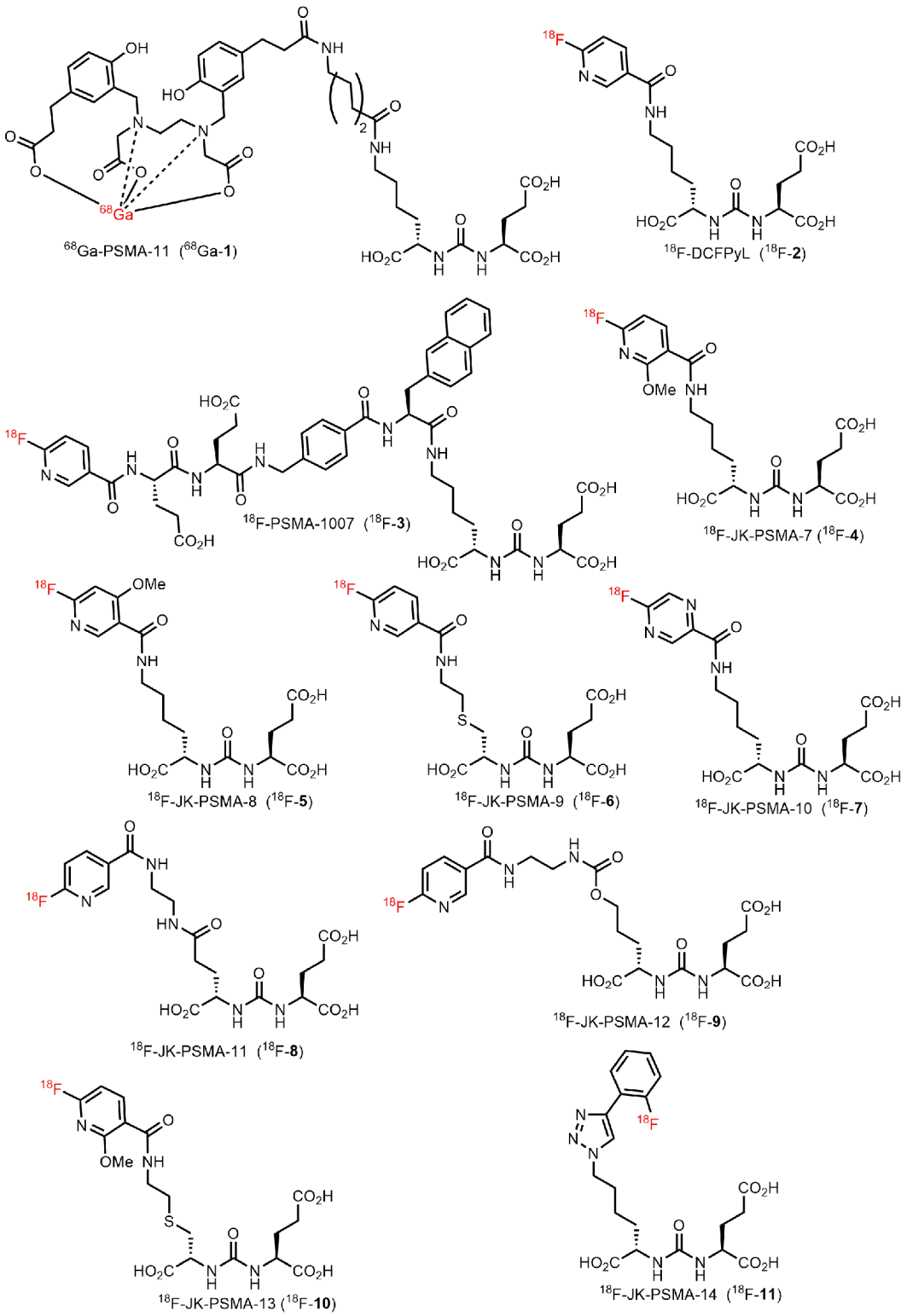

FIGURE 1. Previously known PSMA-specific PET tracers (^{68}Ga-**1**, ^{18}F-**2** and -**3**) and emerging probes (^{18}F-JK-**4**–**11**) investigated in this study.

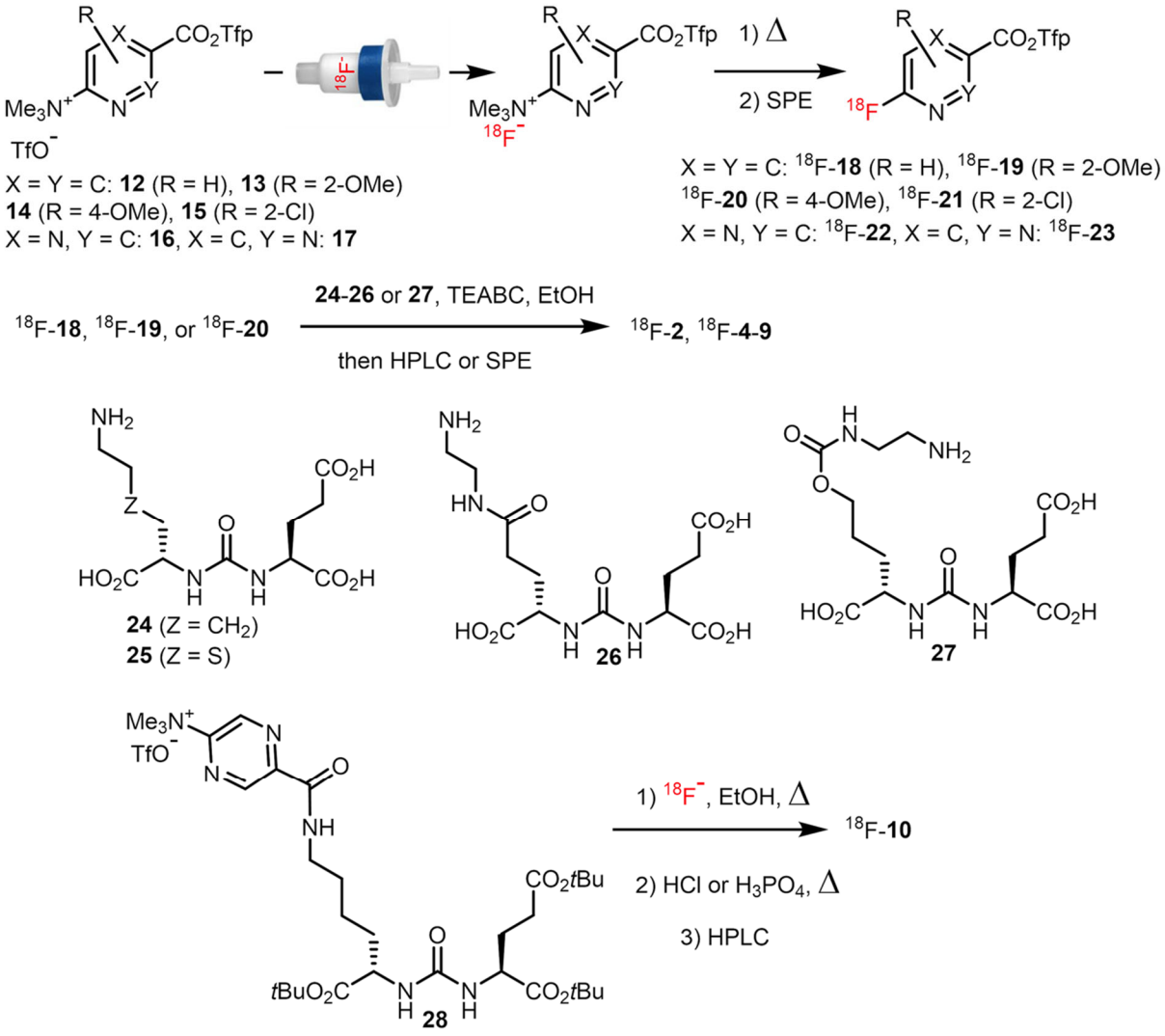

FIGURE 2. Preparation of ^{18}F-**2** and ^{18}F-**4**–**10**.

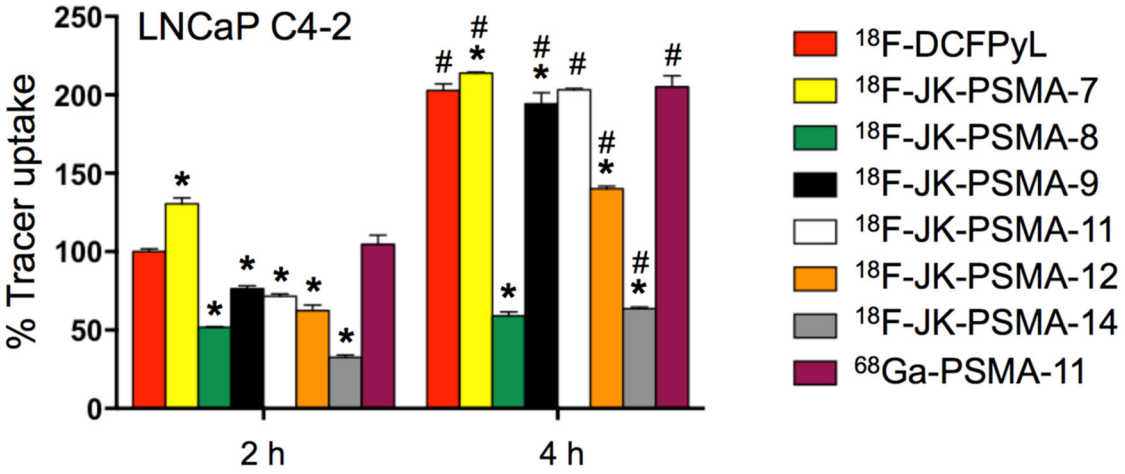

FIGURE 3. Tracer uptake in LNCaP C4-2 cells in relation to ^{18}F-DCFPyL.

^{18}F-DCFPyL uptake after 2 h was normalized to 100%. Only ^{18}F-JK-PSMA-7 shows a higher uptake than ^{18}F-DCFPyL. * Significantly different from ^{18}F-DCFPyL at the same timepoint. $F(7,38)=1136$; $p<0.0001$ for factor „tracer“, post hoc $p<0.05$. # Significantly higher than 2 h-uptake of the same tracer. $F(1,38)=6981$; $p<0.0001$ for factor „time“, post hoc $p<0.05$.

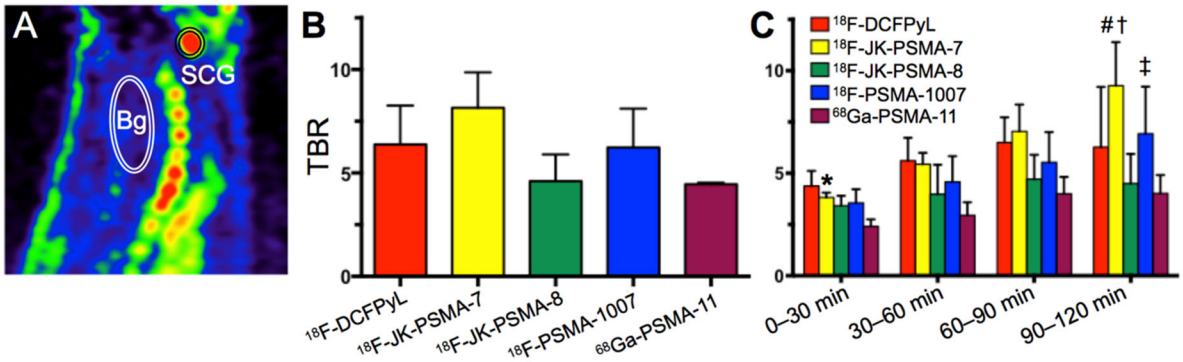

FIGURE 4. Target-to-background ratio (TBR) of PSMA tracers.

A: Sagittal section of a PSMA image with superior cervical ganglion (SCG) and background (Bg) VOIs. B: TBR (SCG/Bg) 60–120 min p.i. was not significantly different between groups [$F(4,10)=2.95$, $p=0.0756$]. C: TBR analyzed for 4×30 min frames. * Significantly higher TBR of ^{18}F-JK-PSMA-7 compared to ^{68}Ga-PSMA-11 [$F(4,40)=5.97$, $p=0.0102$ for factor „tracer“, post hoc $p<0.05$]. # Significantly higher TBR of ^{18}F-JK-PSMA-7 compared to ^{18}F-JK-PSMA-8 and ^{68}Ga-PSMA-11 ($p<0.05$). TBR of ^{18}F-JK-PSMA-7 and ^{18}F-PSMA-1007 increased significantly over time [$F(3,30)=9.12$, $p=0.0002$ for factor „frame“]. † For ^{18}F-JK-PSMA-7, frame 4 was significantly different from frame 1 and 2 ($p<0.05$). ‡ For ^{18}F-PSMA-1007, frame 4 was significantly different from frame 1 ($p<0.05$).

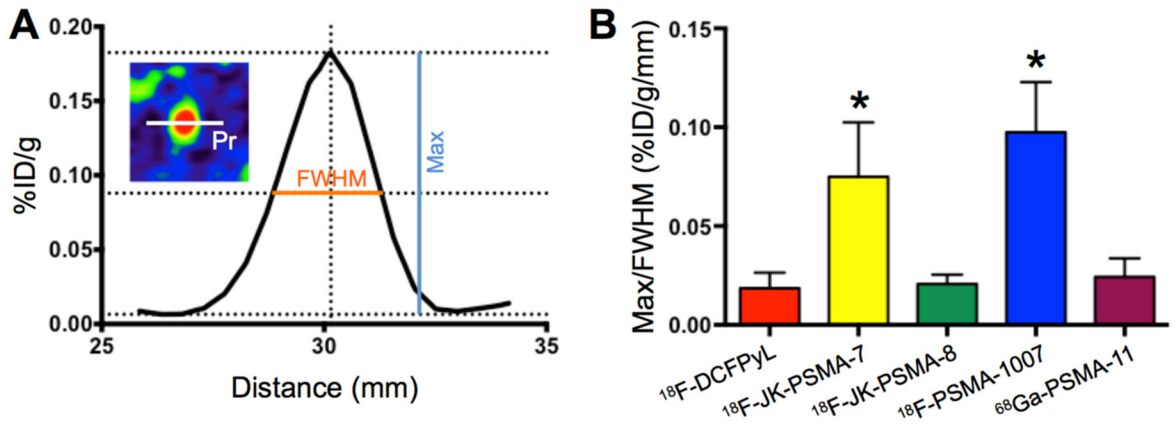

FIGURE 5. Acutance (measured for SCG) using different PSMA tracers.

A: Profile plot of a 1-pixel profile (Pr in insert) through the SCG center. Peak against adjacent background (Max) and full width at half maximum (FWHM) were measured.

B: The ratio Max/FWHM roughly represents the slope of the profile plot and reflects acutance. * ^{18}F-JK-PSMA-7 and ^{18}F-PSMA-1007 show a significantly higher acutance than ^{18}F-DCFPyL, ^{18}F-JK-PSMA-8 and ^{68}Ga-PSMA-11 [$F(4,10)=12.77$, $p=0.0006$; post hoc $p<0.05$].

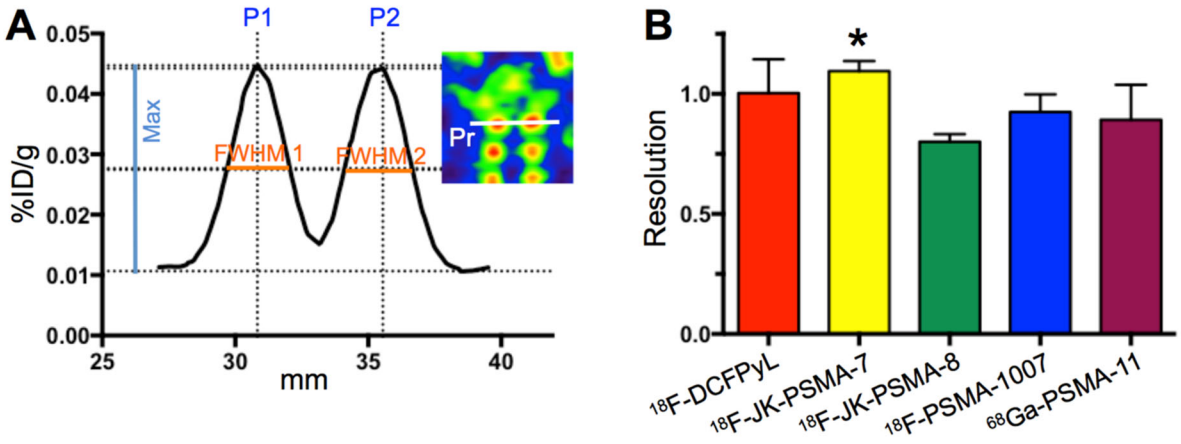

FIGURE 6. Resolution of images acquired with different tracers.

A: Profile plot of a 1-pixel profile (Pr in insert) through the apical pair of DRG. Peak against adjacent background (Max) and full width at half maximum (FWHM) were measured for each ganglion. P2–P1 was the distance between peaks.

B: The formula R=2(P2–P1)/1.7(FWHM1+FWHM2) yields image resolution. * Image resolution was significantly higher for ^{18}F-JK-PSMA-7 compared to ^{18}F-JK-PSMA-8 [$F(4,10)=3.80$, $p=0.0396$, post-hoc $p<0.05$].

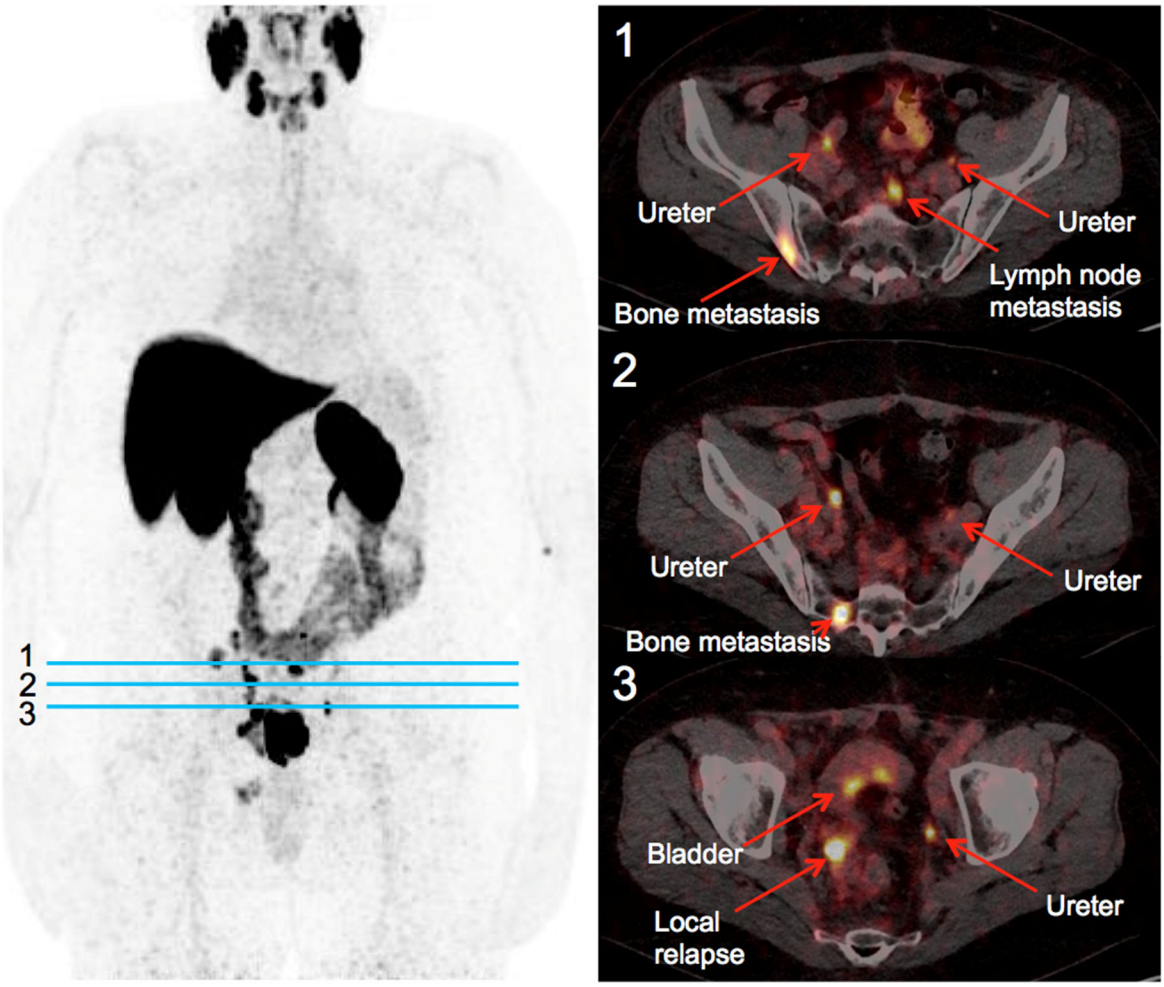

FIGURE 7. ^{18}F-JK-PSMA-7 scan in a patient with relapsed PCa.

The 64 y/o patient had a serum PSA-level of 130 ng/mL. 384 MBq of ^{18}F-JK-PSMA-7 were injected and the scan was started at 233 min p.i.. Left: Maximum intensity projection of the PET image. Right: PET/CT images at transverse levels indicated by blue lines.

TABLE 1. Comparison of quality of PET images obtained with different tracers (60–120 min p.i., n=3).

	Acutance	Resolution	TBR
^{18}F-DCFPyL	0.019±0.008	1.002±0.141	6.38±1.87
^{18}F-JK-PSMA-7	0.075±0.027[a]	1.095±0.042[b]	8.15±1.71
^{18}F-JK-PSMA-8	0.021±0.005	0.800±0.032	4.60±1.30
^{18}F-PSMA-1007	0.097±0.025[a]	0.924±0.074	6.23±1.88
^{68}Ga-PSMA-11	0.024±0.009	0.892±0.146	4.46±0.08

[a] Significantly higher compared to ^{18}F-DCFPyL, ^{18}F-JK-PSMA-8 and ^{68}Ga-PSMA-11 [$F(4,10)=12.77$, $p=0.0006$, post hoc $p<0.05$].
[b] Significantly higher compared to ^{18}F-JK-PSMA-8 [$F(4,10)=3.80$, $p=0.0396$, post hoc $p<0.05$].
TBR: Target-to-background ratio.

TABLE 2. Tracer uptake in different tissues 60–120 min p.i. (n=3 each).

	SCG SUV_{BW}	Sal. gland SUV_{BW}	Liver SUV_{BW}	Blood SUV_{BW}	Bone SUV_{BW}	background SUV_{BW}
^{18}F-DCFPyL	20.9±8.2	13.2±5.3	78.4±29.4	12.9±3.0	10.5±3.5	3.2±0.7
^{18}F-JK-PSMA-7	31.3±10.5	14.4±2.4	119.3±8.3[d]	16.3±4.2	9.9±1.9	4.0±1.0
^{18}F-JK-PSMA-8	14.4±2.6	9.0±2.5	29.0±7.2	8.6±0.3	19.2±2.1	3.2±0.4
^{18}F-PSMA-1007	94.8±19.6[a]	62.1±14.2[b]	50.7±4.3	62.6±10.7[e]	33.2±9.5[g]	15.9±1.7[h]
^{68}Ga-PSMA-11	41.0±3.4	38.4±10.2[c]	43.7±14.4	39.6±4.6[f]	18.5±0.6	9.2±0.6[h]

Sal. gland: salivary gland.

[a] Significantly higher compared to all others. F(4,10)=26.52, p<0.0001, post hoc p<0.05.

[b] Significantly higher compared to all others. F(4,10)=22.06, p<0.0001, post hoc p<0.05.

[c] Significantly higher compared to ^{18}F-DCFPyL. F(4,10)=22.06, p<0.0001, post hoc p<0.05.

[d] Significantly higher compared to ^{18}F-JK-PSMA-8, ^{18}F-PSMA-1007 and ^{68}Ga-PSMA-11. F(4,10)=7.83, p=0.0040, post hoc p<0.05.

[e] Significantly higher compared to all others. F(4,10)=47.59, p<0.0001, post hoc p<0.05.

[f] Significantly higher compared to ^{18}F-DCFPyL, ^{18}F-JK-PSMA-7 and -8. F(4,10)=47.59, p<0.0001, post hoc p<0.05.

[g] Significantly higher compared to all others. F(4,10)=12.19, p=0.0007, post hoc p<0.05.

[h] Significantly different to all others. F(4,10)=93.81, p<0.0001, post hoc p<0.05.

SUPPLEMENTAL DATA

Experimental Setup

The novel PSMA-targeting probes were studied *in vitro* in $PSMA^+$ and $PSMA^-$ prostate cancer cells and in healthy rats with respect to their *in vivo* stability. The metabolic stability of the candidates was determined in healthy rats using μPET. PSMA specificity was determined applying PSMA-expressing peripheral ganglia as a model for small PCa lesions. In a first screening step we selected ^{18}F-JK-PSMA-7 according to its high target-to-background ratio, and, for comparison, its regioisomer, ^{18}F-JK-PSMA-8. Both compounds were compared to ^{18}F-DCFPyL, ^{18}F-PSMA-1007 and ^{68}Ga-PSMA-11 images with respect to biokinetics, biodistribution and the image quality parameters: target-to-background ratio (TBR), acutance and resolution.

Design of the Novel Radiolabeled PSMA Inhibitors

All candidate compounds contain the well-known AA-CO-Glu PSMA binding pharmacophore. JK-PSMA-7, -8 and -10 contain the Lys-CO-Glu, JK-PSMA-9 and -13 – 4-ThiaLys-CO-Glu, JK-PSMA-11 – Glu-CO-Glu, JK-PSMA-12 – 5-(OH)Nva-CO-Glu and JK-PSMA-14 – Nle-CO-Glu motif. JK-PSMA-7–10 and -13 do not contain any spacer and comprise the respective 6-fluronicotinoyl or pyridazinylcarbonyl substituent directly attached to the terminal amino group of the Lys or 4-ThiaLys residue. JK-PSMA-7, -8 and -13 contain a MeO substituent at the 2- or 4-position of the pyridine ring, respectively. JK-PSMA-11 and -12 contain ethylenediamino and ethylendiamino-1-carbonyl spacers attached to the terminal carboxyl and hydroxy groups, respectively. In these cases the 6-fluoronicotinoyl residue is attached to the second amino groups of the spacers. JK-PSMA-14 contains a 1,2,3-triazolyl spacer substituted at the forth position with a 2-fluorophenyl residue."

Synthesis of Precursors for Radiolabeling and Reference Compounds

Onium triflate precursors of radiolabeled active esters **12**–**17** were prepared by the reaction of 2,3,5,6-tetrafluorophenolates of the corresponding 6-chloro-substituted nicotinic acids (**S1**–**4**), 6-chloropyrazine-3-carboxylate (**S5**) or 6-chloropyridazine-3-carboxylate (**S6**) followed by anion metathesis using TMSOTf (Supplemental Fig. 1). The compounds **S1**–**6** were accessed from the appropriate chloroanhydrides (obtained by the treatment of acids **S7**–**12** with oxalyl chloride in the presence of DMF traces) and 2,3,5,6-tetrafluorophenol using Et_3N as a base. Both **S8** and **S9** were prepared from 2,6- and 2,4-dichloronicotinic acids respectively, by the reaction with MeONa, generated *in situ* from MeOH and NaH (*1,2*).

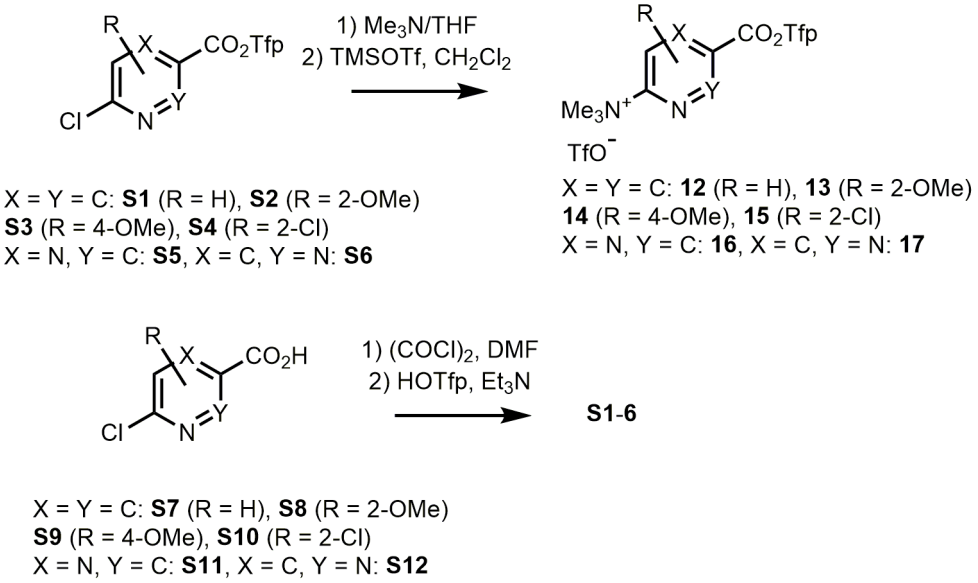

SUPPLEMENTAL FIGURE 1. The preparation of radiolabeling precursors **12**–**17**.

Preparation of precursors for radiolabeling and reference compounds is exemplified in detail for ^{18}F-JK-PSMA-7 and -8.

2,3,5,6-Tetrafluorophenyl 6-chloro-2-methoxynicotinate (6-Cl-2-OMe-Nic-OTfp, S8)

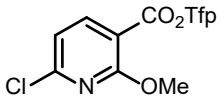

6-Chloro-2-methoxynicotinic acid (**S8**) was prepared according to the literature (*1,3*). To a suspension of this compound (1.87 g, 9.97 mmol) in anhydrous CH_2Cl_2 (10 mL) was added oxalyl chloride (5 mL, 7.4 g, 58.3 mmol) followed by DMF (1 drop, in 5 min an additional drop and in 10 min one more drop). After the vigorous gas evolution had been ceased and the solid completely dissolved, the reaction mixture was concentrated using the argon flow and the residue was dried under reduced pressure affording the respective chloroanhydride (2.5 g, 100% crude) which was immediately used for the next step.

To a solution of this compound in Et_2O (100 mL) was added 2,3,5,6-tetrafluorophenol (1.67 g, 10.06 mmol) followed by Et_3N (1.4 mL, 1.01 g, 10.9 mmol) and the resulting suspension was stirred for 16 h. Afterwards, the reaction mixture was washed with H_2O (3×20 mL), brine (2×20 mL), dried and concentrated under reduced pressure. The residue was recrystallized from hexane affording **S2** (2.4 g, 72%) as a colorless solid.

^{1}H NMR (200 MHz, $CDCl_3$) δ ppm 4.12 (s, 3 H) 7.02 - 7.12 (m, 2 H) 8.38 (d, *J*=8. 0 Hz, 1 H)

^{19}F NMR (188.3 MHz, $CDCl_3$) δ ppm -138.9 (m), -152.5 (m)

^{13}C NMR (50.3 MHz, $CDCl_3$): δ ppm 55.2, 103.40 (t, *J* = 27.9 Hz), 109.0, 116.7, 138.1 (m), 143.5 (m), 144.4, 148.6 (m), 154.6, 159.5, 163.0.

ESI HRMS: calcd for $C_{13}H_5ClF_4NNaO_3^+$: 356.97863; found: 356.97959.

6-Methoxy-*N*,*N*,*N*-trimethyl-5-(2,3,5,6-tetrafluorophenoxycarbonyl)pyridine-2-aminium triflate (6-Me$_3$N^{+-}OTf-2-OMe-Nic-OTfp, 13)

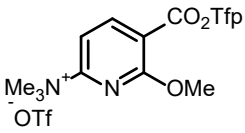

S2 (1.53 g, 4.56 mmol) was dissolved in 2 M NMe_3 in THF (10 mL; stored over CaH_2) and the resulting solution was stirred for 3 h. A colorless solid began to precipitate within the first 5 min. After 3 h, all volatiles were removed at ≤30 °C using the argon flow (under inert atmosphere) and the residue was taken up in anhydrous Et_2O (30 mL) which was removed using the argon flow. The residual solid was carefully washed with anhydrous Et_2O and dried under reduced pressure affording the corresponding chloride salt (1.80 g, 100% crude) as a colorless solid which was immediately used for the next step.

TMSOTf (2.5 mL, 3.04 g, 13.68 mmol) was added to a suspension of the prepared chloride salt (1.8 g, max. 4.56 mmol) in anhydrous CH_2Cl_2 (10 mL) and the mixture was stirred for 30 min. The resulting clear solution was concentrated under reduced pressure and the residue was triturated with Et_2O and recrystallized from EtOAc affording **13** (1.81 g, 78% over two steps) as a colorless solid. The mother liquor was concentrated under reduced pressure and recrystallized from EtOAc giving the second crop of **6** (0.3 g, overall 92%).

^{1}H NMR (200 MHz, DMSO-d_6) δ ppm 2.88 (s, 9 H) 3.38 (s, 3 H) 6.70 (tt, *J*=10.5, 7.3 Hz 1 H) 6.90 (d, *J*=8.2 Hz, 1 H) 8.01 (d, *J*=8.2 Hz, 1 H).

^{19}F NMR (188.3 MHz, DMSO-d_6) δ ppm -155.5 (m), -141.1 (m), -80.05 (m).

^{13}C NMR (50.3 MHz, DMSO-d_6) δ ppm 46.2, 46.7, 95.30, 95.8 (t, *J* = 23.4 Hz), 98.5, 105.1, 109.1, 115.5, 130.1 (m), 135.6 (m), 138.9, 140.6 (m), 149.7 (q, *J* = 45.3 Hz), 154.3.

ESI HRMS: calcd for $C_{16}H_{15}O_3N_2F_4^+$: 359.10133; found: 359.10124.

2,3,5,6-Tetrafluorophenyl 6-chloro-4-methoxynicotinate (6-Cl-4-OMe-Nic-OTfp, S3)

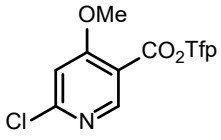

6-Chloro-4-methoxynicotinic acid (**S9**) was prepared according to Ehara et al. (*2*). To a suspension of this compound (3.87 g, 9.97 mmol) in oxalyl chloride (25 mL, 37 g, 291.5 mmol) was added DMF (0.8 mL) followed by anhydrous CH_2Cl_2 (10 mL) and the reaction mixture was stirred 2 h at 60 °C. Afterwards, the reaction mixture was concentrated using the argon flow and the residue was dried under reduced pressure affording the respective chloroanhydride (4.0 g, 100% crude) which was immediately used for the next step.

To a solution of this compound in hot EtOAc (100 mL) was added 2,3,5,6-tetrafluorophenol (2.92 g, 19.35 mmol; vigorous gas evolution was observed). Thereafter, the mixture was cooled to ambient temperature, Et_3N (2.68 mL, 1.96 g, 19.35 mmol) was added dropwise and the resulting suspension was stirred for 1 h. Afterwards, the reaction mixture was washed with H_2O (3×20 mL), brine (2×20 mL), dried and concentrated under reduced pressure. The residue was taken

up in CH_2Cl_2 (70 mL), the suspension was filtered, the filter cake was washed with CH_2Cl_2 (50 mL). The collected dichloromethane fraction was concentrated under reduced pressure. The residue was recrystallized from hexane affording **S3** (2.6 g, 44%) as a colorless solid. The mother liquor was concentrated by reduced pressure and the residue was purified by column chromatography (CH_2Cl_2:hexane=8:2.5) giving the second crop of **S3** (0.8 g, total 58%).

^{1}H NMR (200 MHz, $CDCl_3$) δ ppm 4.04 (s, 3 H) 6.89 - 7.18 (m, 2 H) 8.98 (s, 1 H).

^{1}H NMR (400 MHz, DMSO-d_6) δ ppm 4.04 (s, 3 H) 7.53 (s, 1 H) 8.00 (tt, *J*=10.93, 7.42 Hz, 1 H) 8.90 (s, 1 H).

^{19}F NMR (188.3 MHz, $CDCl_3$) δ ppm -152.4 (m), -138.7 (m).

^{13}C NMR (100.56 MHz, DMSO-d_6) δ ppm 57.5, 104.5, 104.8 (t, *J* = 23.6 Hz), 109.2, 112.0, 128.3 (m), 138.9 (m), 141.3 (m), 144.3 (m), 146.8 (m), 152.9, 157.1, 159.1, 167.1.

ESI HRMS: calcd for $C_{13}H_7ClF_4NO_3^+$: 336.00451; found: 336.00541.

4-Methoxy-*N*,*N*,*N*-trimethyl-5-(2,3,5,6-tetrafluorophenoxycarbonyl)pyridine-2-aminium triflate (6-Me$_3$N$^+$–OTf-4-OMe-Nic-OTfp, 14)

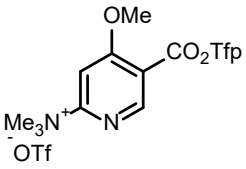

The title compound (1.09 g, 79%; colorless solid) was prepared from **S3** (1.07 g, 2.71 mmol) using 2 M NMe_3 in THF (10 mL; stored over CaH_2) and TMSOTf (1.44 mL, 1.77 g, 17.96 mmol) as described for **13**.

^{1}H NMR (400 MHz, DMSO-d_6) δ ppm 3.65 (s, 9 H) 4.17 (s, 3 H) 7.89 (s, 1 H) 7.96 - 8.13 (m, 1 H) 9.11 (s, 1 H).

^{19}F NMR (188.3 MHz, DMSO-d_6) δ ppm -153.0 (m), -138.8 (m), -77.7 (m).

^{13}C NMR (100.6 MHz, DMSO-d_6) δ ppm 54.7, 58.1, 101.4, 105.0 (t, *J* = 23.6 Hz), 114.3, 120.6 (q, *J* = 241.6 Hz), 128.2 (m), 138.7 (m), 141.2 (m), 144.4 (m), 146.8 (m), 151.6, 158.7, 161.9, 168.51.

ESI HRMS: calcd for $C_{16}H_{15}O_3N_2F_4^+$: 359.10133; found: 359.10262.

2,3,5,6-Tetrafluorophenyl 6-fluoro-2-methoxynicotinate (6-F-2-OMe-Nic-OTfp, 19)

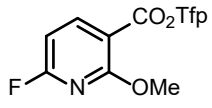

TBAF×4 *t*BuOH (*4*) (0.34 g, 0.59 mmol) was added to a solution of **13** (0.3g, 0.59 mmol) in anhydrous MeCN (2 mL). The resulting solution was mixed for 5 min using the argon flow and diluted with Et_2O (25 mL). The resulting solution was washed with 1 N $NaHSO_4$ (3×10 mL), H_2O (3×10 mL), brine (2×10 mL) and concentrated under reduced pressure. The crude product was purified by column chromatography on C_{18} silica gel (sorbent: RP Chromabond C_{18} ec; Macherey-Nagel, Düren, Germany; eluent: 45% MeCN; dry loading) affording **19** (47 mg, 92% purity, 23%) as a colorless solid.

^{1}H NMR (400 MHz, $CDCl_3$) δ ppm 3.97 - 4.25 (m, 3 H) 6.65 (dd, *J*=8.1, 2.7 Hz, 1 H) 6.92 - 7.16 (m, 1 H) 8.55 (t, *J*=8.1 Hz, 1 H).

^{19}F NMR (376 MHz, $CDCl_3$) δ ppm -152.64 (s), -140.06 (m), -58.74 (m).

^{13}C NMR (100.6 MHz, $CDCl_3$) δ ppm 166.19, 163.0 (d, *J* = 451.7 Hz), 147.5 (d, *J* = 10.6 Hz), 144.8 (m), 142.0 (m), 139.5 (m), 107.6 (d, *J* = 5.3 Hz), 103.4 (t, *J* = 22.1 Hz), 101.1 (d, *J* = 35.2 Hz), 55.2.

ESI HRMS: calcd for $C_{13}H_5F_5NO_3^-$: 318.01951; found: 318.03840.

2,3,5,6-Tetrafluorophenyl 6-fluoro-4-methoxynicotinate (6-F-4-OMe-Nic-OTfp, 20)

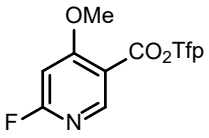

TBAF×4 *t*BuOH (*4*) (0.34 g, 0.59 mmol) was added to a solution of **14** (0.3g, 0.59 mmol) in anhydrous MeCN (2 mL). The resulting solution was mixed for 2 min using the argon flow and diluted with Et_2O (25 mL). The resulting solution was washed with 1 N $NaHSO_4$ (3×10 mL), H_2O (3×10 mL), brine (2×10 mL) and concentrated under reduced pressure. The crude product was purified by column chromatography on C_{18} silica gel (sorbent: RP Chromabond C_{18} ec; Macherey-Nagel, Düren, Germany; eluent: 45% MeCN; dry loading). Fractions containing product were combined and MeCN was removed under reduced pressure. The resulting precipitate was filtered and dried affording **20** (42 mg, 21%) as a colorless solid.

^{1}H NMR (400 MHz, DMSO-d_6) δ ppm 4.03 (s, 3 H) 7.20 (s, 1 H) 7.87 - 8.17 (m, 1 H) 8.83 (s, 1 H).

^{19}F NMR (376 MHz, DMSO-d_6) δ ppm -153.29 - -153.13 (m, 2 F) -139.14- -139.01 (m, 2 F) -58.58 (s, 1 F).

^{13}C NMR (100.6 MHz, DMSO-d_6) δ ppm 170.0 (d, *J* = 12.1 Hz), 168.9, 162.7 (d, *J* = 767.6 Hz), 152.4 (d, *J* = 21.1 Hz), 146.8 (m), 144.4 (m), 141.4 (m), 138.9 (m), 111.5 (d, *J* = 5.0 Hz), 104.8 (t, *J* = 23.6 Hz), 94.5 (d, *J* = 43.3 Hz), 57.6.

ESI HRMS: calcd for $C_{34}H_{58}O_9N_5^+$: 680.42295; found: 680.42228.

5-{[(5*S*)-5-({[(2*S*)-1,5-bis(*tert*-butoxy)-1,5-dioxopentan-2-yl]carbamoyl}amino)-6-(*tert*-butoxy)-6-oxohexyl]carbamoyl}-6-methoxy-*N*,*N*,*N*-trimethyl-pyridine-2-aminium triflate (S13)

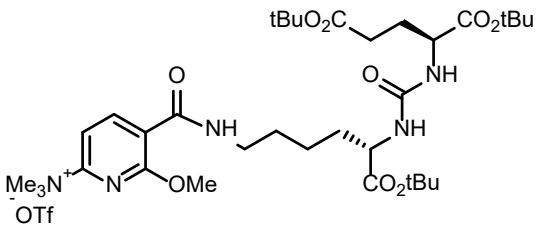

A solution of **13** (0.71 g, 1.4 mmol) and H-Lys-O*t*Bu-ureido-Glu(O*t*Bu)$_2$ (*5*) (0.53 g, 1.09 mmol) in anhydrous CH_2Cl_2 (5 mL) was incubated by ambient temperature for 72 h. The mixture was concentrated under reduced pressure and the residue was purified by column chromatography (first MeCN and, thereafter, CH_2Cl_2:MeOH = 6:1) affording **S13** (0.65 g, 72%) as a colorless foam.

^{1}H NMR (400 MHz, DMSO-d_6) δ ppm 1.26 – 1.32 (m, 2 H) 1.37 (s, 9 H), 1.38 (s, 9 H) 1.39 (s, 9 H) 1.46 - 1.57 (m, 3 H) 1.58 - 1.72 (m, 2 H) 1.79 - 1.94 (m, 1 H) 2.12 - 2.31 (m, 2 H) 3.26 (q, *J*=6.8 Hz, 2 H) 3.57 (s, 9 H) 3.93 - 4.00 (m, 1 H) 4.01 - 4.06 (m, 1 H) 4.04 (s, 3 H) 6.28 (t, *J*=8.7 Hz, 2 H) 7.64 (d, *J*=8.1 Hz, 1 H) 8.34 (d, *J*=7.9 Hz, 1 H) 8.35 (t, *J*=5.7 Hz, 1 H).

^{13}C NMR (100.6 MHz, DMSO-d_6) δ ppm 172.2, 171.9, 171.4, 162.2, 158.9, 157.1, 154.8, 143.5, 120.5, 107.3, 80.6, 80.3, 79.7, 54.9, 54.4, 53.1, 52.1, 39.0, 31.8, 30.9 (×2), 28.6, 27.7, 27.6 (×2), 22.5.

ESI HRMS: calcd for $C_{31}H_{49}O_9N_4FNa^+$: 663.33763; found: 663.33779; calcd for $C_{31}H_{50}O_9N_4F^+$: 641.35513; found: 641.35577.

1,5-Di-*tert*-butyl (2*S*)-2-({[(2*S*)-1-(*tert*-butoxy)-6-[(6-fluoro-2-methoxypyridin-3-yl)formamido]-1-oxohexan-2-yl]carbamoyl}amino)pentanedioate [6-F-2-OMe-Nic-Lys(O*t*Bu)-ureido-Glu(O*t*Bu)$_2$, S14]

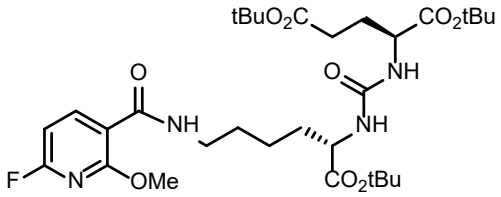

Hexafluorobenzene (82 µL, 132 mg, 0.71 mmol) was added dropwise to a solution of Bu_4NCN (1.15 g, 4.26 mmol) in anhydrous MeCN (4.3 mL), the resulting dark-red solution was stirred for 40 min and added to the above triflate (0.59 g, 0.71 mmol). The resulting mixture was stirred for 16 h and taken up with Et_2O and H_2O (50 mL of each). The ethereal layer was separated and washed with H_2O (3×20 mL), brine (2×20 mL), dried and concentrated under reduced pressure. The residue was purified by column chromatography (Et_2O) and sonication with pentane to give **S14** (0.31 g, 68%) as a viscous yellow oil. R_f=0.36 (EtOAc:hexane=1:1).

^{1}H NMR (300 MHz, $CDCl_3$) δ ppm 1.10 - 1.31 (m, 1 H) 1.42 (s, 9 H) 1.44 (s, 9 H) 1.44 (s, 9 H) 1.46 - 1.52 (m, 1 H) 1.55 - 1.73 (m, 3 H) 1.75 - 1.93 (m, 2 H) 1.97 - 2.17 (m, 1 H) 2.18 - 2.45 (m, 2 H) 3.43 (d, *J*=6.3, 19.6 Hz, 2 H) 4.08 (s, 3 H) 4.20 - 4.45 (m, 2 H) , 4.79 - 5.78 (br, 2 H) 6.62 (dd, *J*=8.2, 3.1 Hz, 1 H) 7.76 (t, *J*=5.50 Hz, 1 H) 8.63 (t, *J*=8.2 Hz, 1 H).

^{19}F NMR (282 MHz, $CDCl_3$) δ ppm -65.45 (dd, *J*=8.2, 2.7 Hz).

^{13}C NMR (75.5 MHz, $CDCl_3$): δ ppm 22.5, 27.95, 27.97, 28.03, 28.5, 29.1, 31.5, 32.3, 39.3, 52.9, 53.4, 54.9, 80.5, 81.6, 81.9, 101.7 (d, *J* = 35.5 Hz), 113.2 (d, *J* = 5.3 Hz), 146.9 (t, *J* = 9.1 Hz), 156.9, 159.9 (d, *J* = 14.3 Hz), 162.8 (d, *J* = 246.9 Hz), 163.0, 172.0, 172.3, 172.4.

ESI HRMS: calcd for $C_{31}H_{49}O_9N_4FNa^+$: 663.33763; found: 663.33779; calcd for $C_{31}H_{50}O_9N_4F^+$: 641.35513; found: 641.35577.

(2*S*)-2-({[(1*S*)-1-carboxy-5-[(6-fluoro-2-methoxypyridin-3-yl)formamido]-pentyl]carbamoyl}amino)pentanedioic acid (4, JK-PSMA-7)

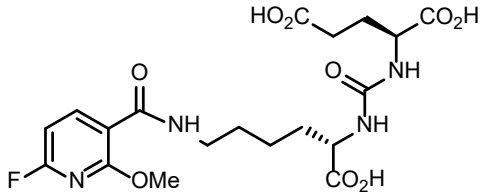

A solution of **S14** (0.31 g, 0.66 mmol) in TFA/TIS/H_2O=95/2.5/2.5 (10 mL) was incubated for 90 min at ambient temperature. Afterwards, all volatiles were removed under reduced pressure and the residue was taken up in TFA (10 mL), the resulting solution was incubated at ambient temperature for 3 h and concentrated under reduced pressure. The

residue was sonicated with Et_2O (×5) and recrystallized from MeOH/Et_2O affording **4** (80 mg, 36%) as a colorless solid. The mother liquor was concentrated under reduced pressure and the residue was recrystallized from MeOH/Et_2O to give the second crop of the title compound (45 mg, overall 56%).

^{1}H NMR (300 MHz, CD_3OD) δ ppm 1.43 - 1.57 (m, 2 H) 1.58 - 1.80 (m, 3 H) 1.81 - 1.98 (m, 2 H) 2.07 - 2.22 (m, 1 H) 2.32 - 2.49 (m, 2 H) 3.41 (t, *J*=6.87 Hz, 2 H) 4.06 (s, 3 H) 4.22 - 4.37 (m, 2 H) 6.70 (dd, *J*=8.15, 2.89 Hz, 1 H) 8.39 (t, *J*=8.15 Hz, 1 H).

^{19}F NMR (282 MHz, CD_3OD) δ ppm -67.67 (dd, *J*=7.80, 3.04 Hz).

^{13}C NMR (75.5 MHz, CD_3OD): δ (ppm) 24.2, 29.1, 30.2, 31.2, 33.3, 40.8, 53.7, 54.2, 55.5, 102.3 (d, *J* = 36.2 Hz), 115.2 (d, *J* = 5.3 Hz), 147.1 (d, *J* = 9.1 Hz), 160.3, 161.9 (d, *J* = 14.3 Hz), 162.94 165.71 (d, *J* = 209.1 Hz), 166.2, 175.9, 176.5, 176.6.

ESI HRMS: calcd for $C_{19}H_{25}O_9N_4FK^+$: 511.12372; found: 511.12366; calcd for $C_{19}H_{25}O_9N_4FNa^+$: 495.14978; found: 495.14959; calcd for $C_{19}H_{26}O_9N_4F^+$: 473.16784; found: 473.16756.

5-{[(5*S*)-5-({[(2*S*)-1,5-Bis(*tert*-butoxy)-1,5-dioxopentan-2-yl]carbamoyl}amino)-6-(*tert*-butoxy)-6-oxohexyl]carbamoyl}-4-methoxy-*N*,*N*,*N*-trimethyl-pyridine-2-aminium triflate (S15)

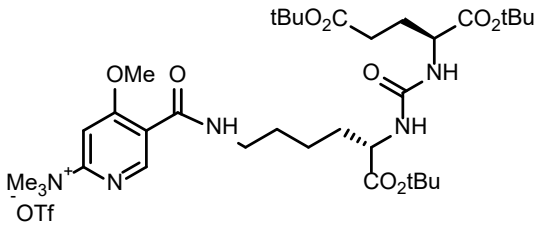

2,4,6-Trimethylpyridine (0.295 mL, 0.27 g, 2.23 mmol) was added to a solution of **14** (0.454 g, 0.89 mmol) and H-Lys-O*t*Bu-ureido-Glu(O*t*Bu)$_2$ (*5*) (0.435 g, 0.89 mmol) in anhydrous CH_2Cl_2 (5 mL) and the reaction mixture was incubated by ambient temperature for 3 h and diluted with Et_2O (70 mL). The precipitated crude product was recrystallized from CH_2Cl_2/Et_2O (×2) and MeCN/Et_2O, concentrated under reduced pressure and, finally purified by column chromatography on C_{18} silica gel [sorbent: Sep-Pak C_{18}; Waters GmbH, Eschborn, Germany; eluent: 35% MeCN (0.1% TFA) until polar impurities completely eluted (HPLC control), thereafter column dried with air before product was eluted with MeCN; dry loading] affording **S15** (0.57 g, 79%, mixture of the corresponding TFA and TFMSA salts ca. 1:1) as a colorless foam.

^{1}H NMR (400 MHz, DMSO-d_6) δ ppm 1.28 - 1.36 (m, 2 H) 1.39 (s, 18 H) 1.40 (s, 9 H) 1.46 - 1.59 (m, 3 H) 1.59 - 1.73 (m, 2 H) 1.80 - 1.93 (m, 1 H) 2.14 - 2.31 (m, 2 H) 3.25 (q, *J*=6.71 Hz, 2 H) 3.59 (s, 9 H) 3.94 - 4.00 (m, 1 H) 4.01 – 4.06 (m, 1 H) 4.06 (s, 3 H) 6.29 (d, *J*=8.0 Hz, 1 H) 6.31 (d, *J*=8.0 Hz, 1 H) 7.71 (s, 1 H) 8.36 (t, *J*=5.69 Hz, 1 H) 8.58 (s, 1 H).

^{19}F NMR (376 MHz, DMSO-d_6) δ (ppm) -73.63 (TFA), -77.76 (TFMSA).

^{13}C NMR (100.6 MHz, DMSO-d_6) δ ppm 172.3, 171.9, 171.4, 165.5, 162.1, 159.2, 157.1, 148.5, 122.6, 99.8, 80.6, 80.3, 79.7, 57.3, 54.7, 53.1, 52.1, 38.9, 31.7, 30.9 (×2), 28.6, 27.7 (×2), 27.6, 22.5.

ESI HRMS: calcd for $C_{34}H_{58}O_9N_5^+$: 680.42291; found: 680.42240.

1,5-Di-*tert*-butyl (2*S*)-2-({[(2*S*)-1-(*tert*-butoxy)-6-[(6-fluoro-4-methoxypyridin-3-yl)formamido]-1-oxohexan-2-yl]carbamoyl}amino)pentanedioate (6-F-4-OMe-Nic-Lys(O*t*Bu)-ureido-Glu(O*t*Bu)$_2$, S16)

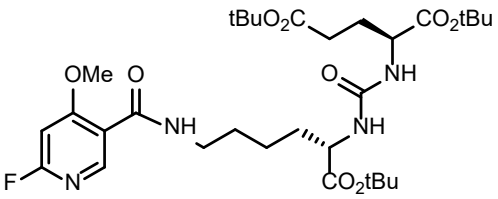

A solution of **S15** (0.41 g, 0.494 mmol) and TBAF×4 *t*BuOH (*4*) (0.69 g, 1.24 mmol) in anhydrous MeCN (1 mL) was incubated at ambient temperature for 3 h, and diluted with Et_2O and 1 N $NaHSO_4$ (50 mL of each). The organic fraction was separated, washed with 1 N $NaHSO_4$ (3×10 mL), H_2O (3×10 mL), brine (2×10 mL), dried and concentrated under reduced pressure. The crude product was purified by column chromatography (EtOAc) affording **S16** (0.27 g, 85%) as a colorless foam.

^{1}H NMR (400 MHz, $CDCl_3$) δ ppm 1.25 - 1.51 (m, 2 H) 1.43 (s, 9 H) 1.44 (s, 9 H) 1.45 (s, 9 H) 1.55 - 1.73 (m, 3 H) 1.74 - 1.91 (m, 2 H) 1.99 - 2.12 (m, 1 H) 2.20 - 2.41 (m, 2 H) 3.40 - 3.48 (m, 2 H) 4.05 (s, 3 H) 4.27 - 4.39 (m, 2 H) 4.51 - 5.66 (br, 2 H) 6.47 (s, 1 H) 7.41 (t, *J*=5.44 Hz, 1 H) 8.88 (s, 1 H).

^{19}F NMR (376 MHz, $CDCl_3$) δ ppm -61.66 (s).

^{13}C NMR (100.6 MHz, $CDCl_3$) δ ppm 172.5, 172.3, 172.0, 166.7 (d, *J*=22.1 Hz), 165.3 (d, *J*=240.4 Hz), 162.9, 156.9, 152.4 (d, *J*=19.1 Hz), 116.5, 91.9 (d, *J*=42.3 Hz), 82.1, 81.8, 80.6, 56.7, 53.4, 53.0, 39.4, 32.6, 31.5 (×2), 29.0, 28.4, 28.04, 27.96 (×2), 22.6.

ESI HRMS: calcd for $C_{31}H_{50}O_9N_4F^+$: 641.35513; found: 641.35547.

(2*S*)-2-({[(1*S*)-1-carboxy-5-[(6-fluoro-4-methoxypyridin-3-yl)formamido]-pentyl]carbamoyl}amino)pentanedioic acid (5, JK-PSMA-8)

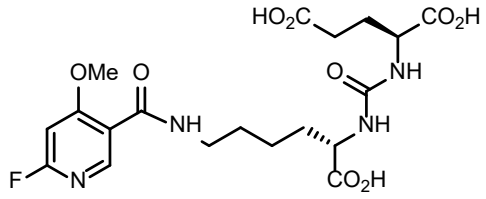

A solution of **S16** (0.26 g, 0.42 mmol) in TFA/TIS/H_2O=95/2.5/2.5 (2 mL) was incubated for 90 min at ambient temperature. Afterwards, all volatiles were removed under reduced pressure and the residue was taken up in TFA (10 mL), the resulting solution was incubated at ambient temperature for 3 h, filtered and concentrated under reduced pressure. The residue was sonicated with Et_2O (×5) and recrystallized from acetone/Et_2O affording **1** (170 mg, 85%) as a colorless solid.

^{1}H NMR (400 MHz, CD_3OD) δ ppm 1.50 (q, *J*=7.67 Hz, 2 H) 1.58 - 1.79 (m, 3 H) 1.80 - 1.98 (m, 2 H) 2.14 (dd, *J*=13.38, 5.88 Hz, 1 H) 2.31 - 2.51 (m, 2 H) 3.40 (t, *J*=6.88 Hz, 2 H) 4.05 (s, 3 H) 4.25 - 4.35 (m, 2 H) 6.84 (s, 1 H) 8.47 (s, 1 H).
^{19}F NMR (376 MHz, CD_3OD) δ ppm -65.34 (s).
^{13}C NMR (100.6 MHz, CD_3OD) δ ppm 176.62, 176.55, 176.0, 169.2 (d, *J*=11.1 Hz), 167.9 (d, *J*=239.4 Hz), 165.7, 160.3, 150.8 (d, *J*=18.1 Hz), 119.8 (d, *J*=5.0 Hz), 93.9 (d, *J*=42.3 Hz), 57.8, 54.2, 53.6, 40.8, 33.4, 31.3, 30.1, 29.1, 24.2.
ESI HRMS: calcd for $C_{19}H_{25}O_9N_4FNa^+$: 495.14978; found: 495.14985; calcd for $C_{19}H_{26}O_9N_4F^+$: 473.16784; found: 473.16775.

Production of ^{18}F-fluoride

^{18}F-Fluoride was produced by the ^{18}O(p,n)^{18}F reaction by bombardment of enriched ^{18}O-water with 16.5 MeV protons using a MC16 cyclotron (Scanditronix, Sweden) at the Max Planck Institute for Metabolism Research (Cologne) or a BC1710 cyclotron (The Japan Steel Works Ltd., Japan) at the INM-5 (Forschungszentrum Jülich).

Manual Synthesis of ^{18}F-JK-PSMA-7 (^{18}F-4)

Aqueous ^{18}F-fluoride (0.05–50 GBq) was loaded onto a Sep-Pak Accell Plus QMA carbonate plus light cartridge (Waters GmbH, Eschborn, Germany; preconditioned with 1 mL H_2O). The resin was washed with anhydrous EtOH (3 mL) and ^{18}F-fluoride was eluted into the reaction vessel with a solution **13** (10 mg, 21 µmol) in anhydrous EtOH (200 µL). The resin was flushed with anhydrous MeCN/*t*BuOH 1:4 (2 mL) into the reaction vessel. The mixture was allowed to stir at 45 °C for 15–20 min. After that, the crude mixture was diluted with water (10 mL) and the solution was loaded onto a polymer RP or C-18 cartridge. The cartridge was washed with water (10 mL) and ^{18}F-**19** was eluted with EtOH (500 µL). Alternatively, the anion exchange resin was washed with anhydrous MeCN (3 mL) and ^{18}F-fluoride was eluted into the reaction vessel with a solution of **13** (12 mg, 25 µmol), in anhydrous MeCN/*t*BuOH 1:4 (0.6 mL). The resin was flushed with anhydrous MeCN/*t*BuOH 1:4 (1 mL) into the reaction vessel. The mixture was allowed to stir at 40 °C for 1–3 min, diluted with water (10 mL) and the solution was loaded onto a polymer RP or C-18 cartridge.
The cartridge was washed with water (10 mL), ^{18}F-**19** was eluted with EtOH (500 µL) directly to a solution of Lys-C(O)-Glu (**24**) (2.5 mg, 7.8 µmol) in 0.19 M Et_4NHCO_3 in anhydrous EtOH (160 µL) and the reaction mixture was allowed to stir for 3–5 min at 45 °C. The mixture was quenched with 0.1% TFA (20 mL) and loaded onto a Sep-Pak C_{18} plus long cartridge [Waters GmbH, Eschborn, Germany; preconditioned with EtOH (2 mL) followed by H_2O (10 mL)]. The cartridge

was washed with H_2O (10 mL) and after that plugged to an Oasis HLB plus short cartridge (Waters GmbH, Eschborn, Germany). ^{18}F-**4** was transferred from the C_{18} onto the HLB resin by 1.7% H_3PO_4 in 6% EtOH (60 mL). HLB cartridge was washed with H_2O (10 mL) and ^{18}F-JK-PSMA-7 (18–22% n.d.c.) eluted with 50% EtOH in isotonic saline (2 mL). Quality control: eluent: 10% EtOH (1.7% H_3PO_4) for 5 min, then 50% EtOH for 2 min. Flow rate: 3 mL/min. Column: Chromolith® SpeedROD RP-18e column (Merck, Darmstadt Germany), 50×4.6 mm. Retention times: ^{18}F-**4** =3 min; ^{18}F-**19** = 5.7 min.

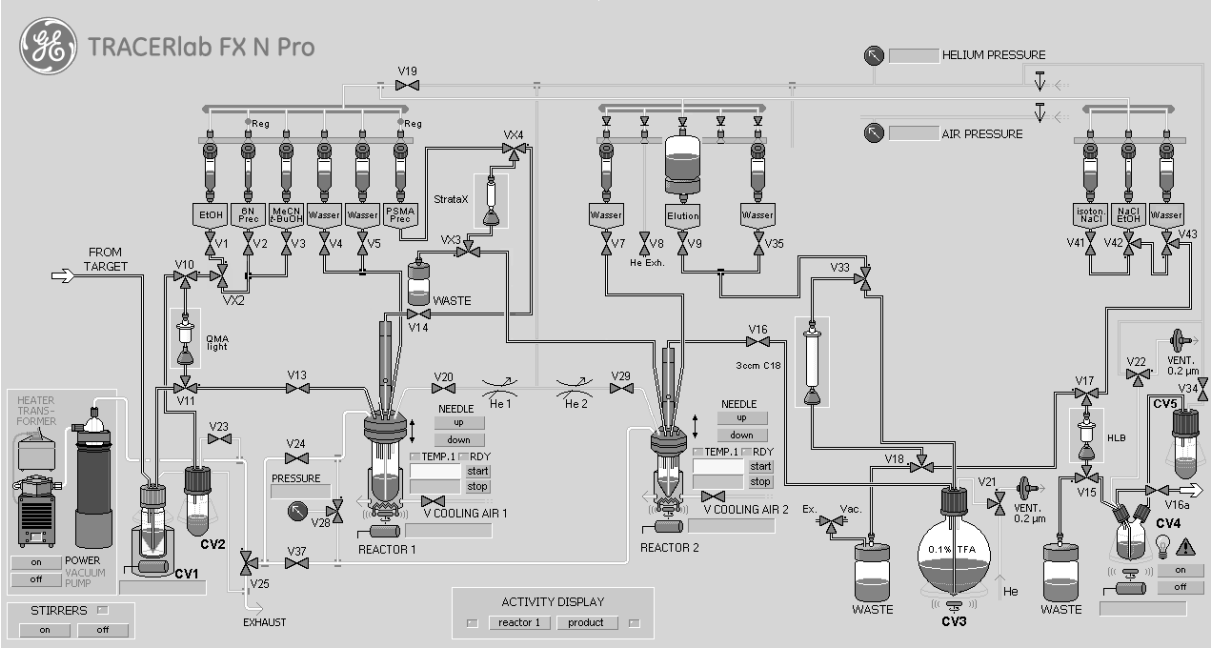

SUPPLEMENTAL FIGURE 2. Process flow diagram (PFD) for the automated radiosynthesis of ^{18}F-JK-PSMA-7 on FXNPro module (GE).

Automated Production of ^{18}F-4 on FXNPro Module (GE) (Supplemental Fig. 2)

Aqueous ^{18}F-fluoride (30–50 GBq) was transferred from the cyclotron target into a trapping vial and thereafter loaded onto a anion-exchange resin cartridge (Sep-Pak QMA carbonate light 46 mg; preconditioned with 1 mL water) from the male side of the cartridge. ^{18}O-H_2O was collected in a separate vial. The cartridge was subsequently washed with MeCN (4 mL) from vial V1 from the female side of the cartridge. The resulting washings were discarded. Thereafter, ^{18}F-fluoride was slowly eluted from the resin with a solution of **13** (10 mg, 21 µmol) in MeCN/*t*BuOH 1:4 (1 mL) from the vial V2 into reactor RI using a stream of He. Afterwards, MeCN (2 mL) from vessel V3 was passed through the cartridge into reactor RI. Reactor RI was filled with He, sealed and the reaction mixture was heated at 45 °C for 3 min. After cooling to ambient temperature the reaction mixture was diluted with H_2O (15 mL) from vessel V5 and loaded onto a polymer RP

cartridge (Strata X, Phenomenex, Aschaffenburg, Germany; preconditioned with 1 mL EtOH followed by 5 mL H_2O). The cartridge was washed with H_2O (10 mL) from vial V4 and dried using a flow of He for 5 min.

^{18}F-**19** was eluted with a freshly prepared solution of Lys-C(O)-Glu (**24**) (4.6 mg, 15.2 µmol) and Et_4NHCO_3 (11.6 mg, 60.6 µmol) in EtOH (1 mL) from vial VX4 into reactor R2. The reaction mixture was heated at 40 °C for 3 min. After cooling to ambient temperature the reaction mixture was diluted with water (1 mL) from vial V7 and transferred to vessel CV3 containing 0.1% TFA (20 mL). The acidic solution was loaded onto a Sep-Pak tC_{18} Plus Long Cartridge 900 mg (Waters GmbH, Eschborn, Germany; preconditioned with 10 mL EtOH followed by 30 mL H_2O). The cartridge was subsequently washed with water (10 mL) from vial V35 and ^{18}F-**4** was eluted with 1.7% H_3PO_4 in 12% EtOH (60 mL) onto a HLB catridge (Oasis HLB Plus Short Cartridge 225 mg, Waters GmbH, Eschborn, Germany; preconditioned with 10 mL EtOH followed by 30 mL H_2O) from vessel V9. The HLB cartridge was washed with 10 mL water from vessel V43 with a flow of helium for 1 min and the purified ^{18}F-**4** was eluted with 50% EtOH in isotonic saline (2 mL). The resulting solution was diluted with isotonic saline (9 mL) and sterile filtered. Alternatively, the crude ^{18}F-**4** was diluted with sodium phosphate buffer {3 mL; 1 L of the buffer was prepared by dilution of 2 mL 85% H_3PO_4 and sodium phosphate buffer concentrate [20 mL; contains Na_2HPO_4×12 H_2O (Ph. Eur.) 3.05 g and NaH_2PO_4×2 H_2O (Ph. Eur.) 0.462 g, B. Braun Melsungen AG, Melsungen, Germany] to 1 L} and loaded onto preparative HPLC. Conditions: Column: Prontosil 120-5 C_{18} ace EPS 250×20 mm (BISCHOFF Analysentechnik u. -geräte GmbH, Leonberg, Germany); Eluent: 30% MeCN in sodium phosphate buffer {1 L of the buffer was prepared by dilution of 2 mL 85% H_3PO_4 and sodium phosphate buffer concentrate [20 mL; contains Na_2HPO_4×12 H_2O (Ph. Eur.) 3.05 g and NaH_2PO_4×2 H_2O (Ph. Eur.) 0.462 g, B. Braun Melsungen AG, Melsungen, Germany] to 1 L}; Flow rate: 15 mL/min; Detection: 220 nm. Fraction containing the purified tracer was diluted with H_2O (10 mL) and loaded onto a HLB catridge (Oasis HLB Plus Short Cartridge 225 mg, Waters GmbH, Eschborn, Germany; preconditioned with 10 mL EtOH followed by 30 mL H_2O) from vessel V9. The HLB cartridge was washed with 10 mL water from vessel V43 with a flow of helium for 1 min and the purified ^{18}F-**4** was eluted with 50% EtOH in isotonic saline (2 mL). The resulting solution was diluted with isotonic saline (9 mL) and sterile filtered. Quality control: see above. ^{18}F-JK-PSMA-7 was prepared in a RCY of 18–25% (n.d.c.) and with molar activity of 75–120 GBq/µmol.

Cultivation of Cells

PSMA$^-$ PC-3 and PSMA$^+$ LNCaP C4-2 prostate tumor cells were generous gift of G. Winter (Ulm, Germany). PC-3 cells were cultured in RPMI-1640 medium supplemented with FBS (10%)

and penicillin/streptomycin (1%). $PSMA^+$ LNCaP C4-2 cells were cultured in a mixture of DMEM: Ham's F-12K (Kaighn's) mediums (4:1) supplemented with FBS (5%), NaHCO3 (3 g/L), insulin (5 µg/mL), triiodothyronine (13.6 pg/mL), transferrin (5 µg/mL), biotin (0.25 µg/ml) and adenine (25 µg/mL). Both cell lines were grown in 75 mL flasks containing 10 mL of the culture medium in a humidified atmosphere of 5% CO_2/95% air at 37 °C for 4–5 days until they reached 80–90% confluency. Cells were seeded into 12-well plates (1×10^5 cells/well containing 1 mL medium) 24 h before the beginning of the cellular uptake experiments.

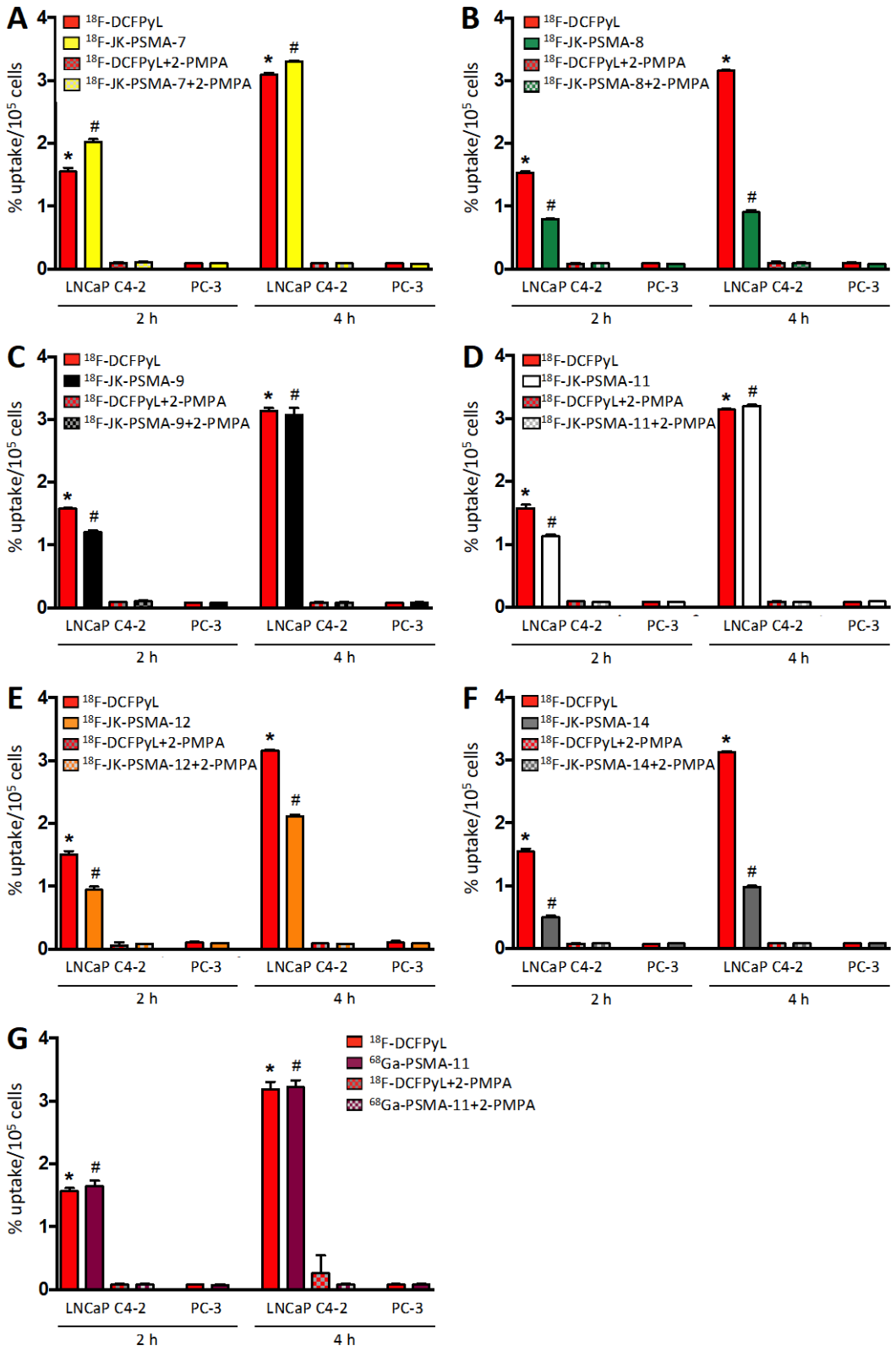

SUPPLEMENTAL FIGURE 3. Figure legend see next page.

SUPPLEMENTAL FIGURE 3. Cellular uptake of the novel PSMA tracers compared to that of ^{18}F-DCFPyL. A: ^{18}F-JK-PSMA-7, B: ^{18}F-JK-PSMA-8, C: ^{18}F-JK-PSMA-9, D: ^{18}F-JK-PSMA-11, E: ^{18}F-JK-PSMA-12, F: ^{18}F- JK-PSMA-13, G: ^{68}Ga-PSMA-11. *,$^{\#}$: Significantly different from all other values of the same timepoint. Exceptions: Uptake of ^{18}F-DCFPyL and ^{18}F-JK-PSMA-9 in LNCaP C4-2 cells was not significantly different after 4 h (C). Uptake of ^{18}F-DCFPyL and ^{68}Ga-PSMA-11 in LNCaP C4-2 cells was not significantly different after 2 h and after 4 h (G). For detailed statistical results see Supplemental Table 1.

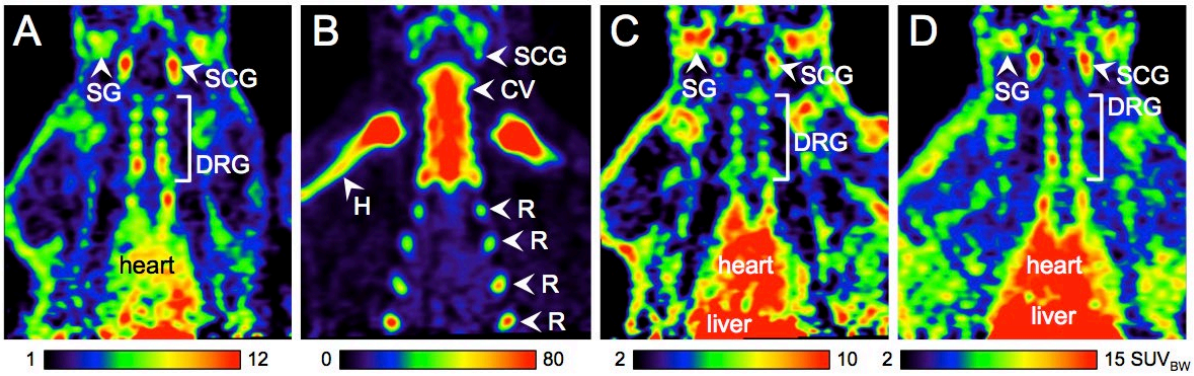

SUPPLEMENTAL FIGURE 4. Biodistribution of discontinued PSMA-tracers.

These tracers were tested only once in the same animal and were not further evaluated because of insufficiently high target-to-background ratio. A: ^{18}F-JK-PSMA-9. B: ^{18}F-JK-PSMA-10, showing substantial defluorination associated with high bone uptake. C: ^{18}F-JK-PSMA-11. D: ^{18}F-JK-PSMA-13. Abbreviations: CV: cervical vertebrae, DRG: dorsal root ganglia, H: humerus, R: ribs, SG: salivary gland, SCG: superior cervical ganglion.

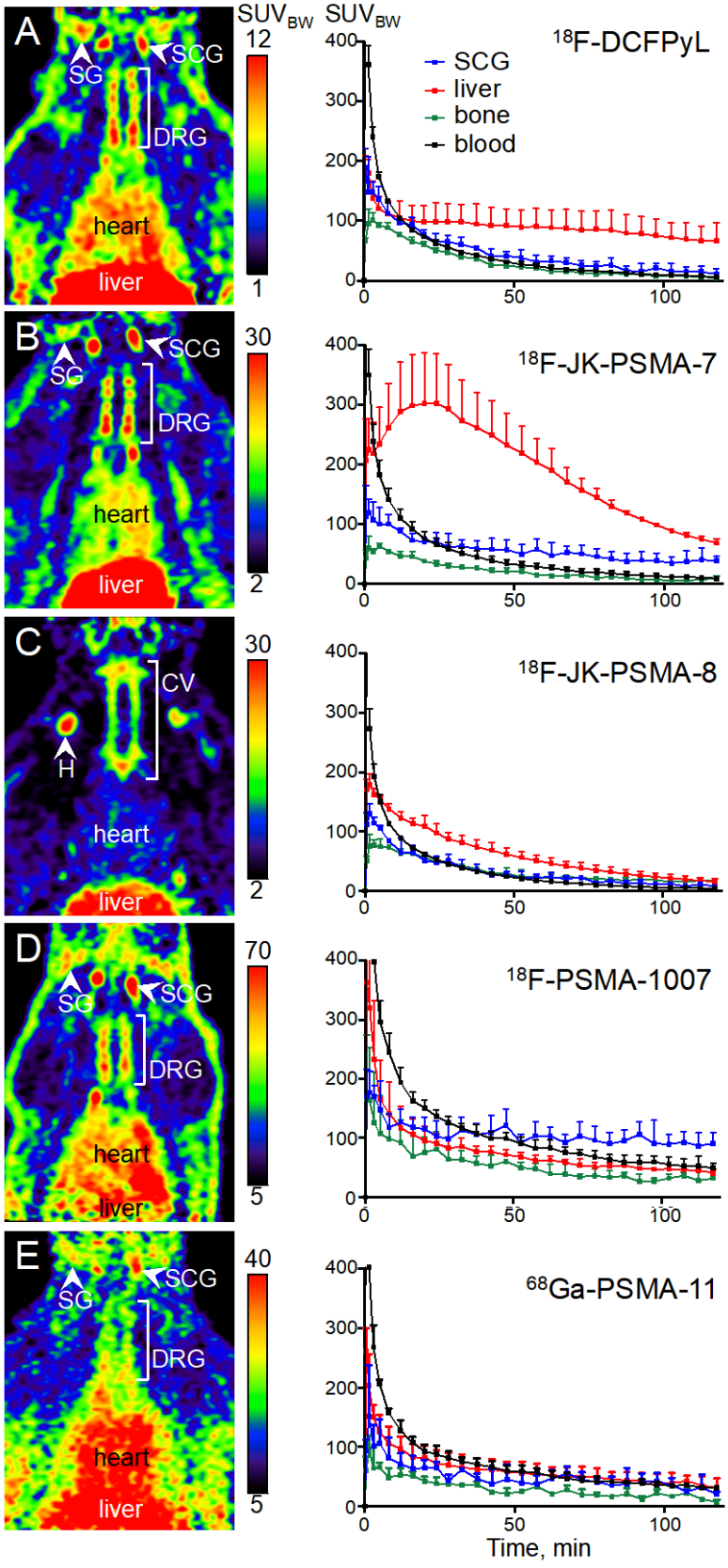

SUPPLEMENTAL FIGURE 5. Figure legend see next page.

SUPPLEMENTAL FIGURE 5. Biodistribution and kinetics of PSMA tracers.

Shown are PET images in horizontal orientation together with time-activity-curves (TACs) of SCG, liver, bone (sternum) and blood (input function, see Supplemental Fig. 6) measured with ^{18}F-DCFPyL (A), ^{18}F-JK-PSMA-7 (B), ^{18}F-JK-PSMA-8 (C), ^{18}F-PSMA-1007 (D) and ^{68}Ga-PSMA-11 (E). While the TACs all have the same scale (0–400 SUV_{BW}), image intensity has been individually adjusted for optimal presentation. Abbreviation: CV: cerebral vertebrae, DRG: dorsal root ganglia, H: humeral head, SCG: superior cervical ganglion, SG: salivary gland.

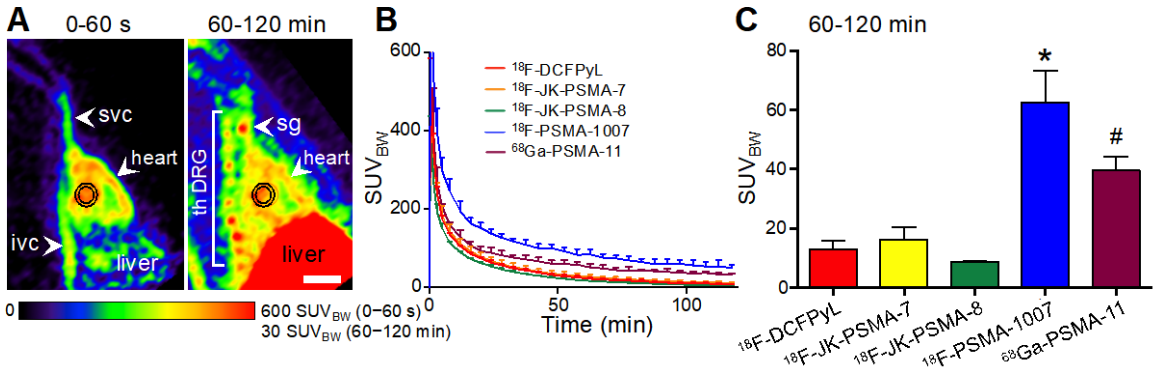

SUPPLEMENTAL FIGURE 6. PSMA-tracer input functions (n=3 each)

A: Sagittal sections of early (0–60 s) and late (60–120 min) time frames from the same ^{18}F-DCFPyL scan. Blood radioactivity concentration was measured in the heart (VOI: black circle). Scale bar: 1 cm. B: Blood time-activity-curves (=input function) of different PSMA-tracers. Blood radioactivity of ^{18}F-PSMA-1007 was highest at all times. C: Quantification of the frame 60−120 min after injection. * Blood radioactivity of ^{18}F-PSMA-1007 was significantly higher compared to all other tracers [$F(4,10)=47.59$, $p<0.0001$, post hoc $p<0.05$]. # Blood radioactivity of ^{68}Ga-PSMA-11 was significantly higher compared to ^{18}F-DCFPyL, ^{18}F-JK-PSMA-7 and -8 (post hoc $p<0.05$). Abbreviations: ivc: inferior vena cava; sg: stellate ganglion; svc: superior vena cava; th DRG: thoracic dorsal root ganglia.

SUPPLEMENTAL TABLE 1: Statistical results of individual cell uptake studies, 2-way ANOVA followed by Sidak's multiple comparison test.

Tracer	Main effect of factor "tracer/cell line/inhibitor" *	Main effect of factor "time" **	LNCaP C4-2: Tracer vs. ^{18}F-DCFPyL	Tracer (LNCaP C4-2) vs. all others #	LNCaP C4-2: 2 h vs. 4 h
^{18}F-JK-PSMA-7	F(5,24)=17272 p<0.0001	F(1,24)=3615 p<0.0001	2 h: p<0.05 4 h: p<0.05	2 h: p<0.05 4 h: p<0.05	^{18}F-JK-PSMA-7: p<0.05 ^{18}F-DCFPyL: p<0.05
^{18}F-JK-PSMA-8	F(5,24)=20177 p<0.0001	F(1,24)=3155 p<0.0001	2 h: p<0.05 4 h: p<0.05	2 h: p<0.05 4 h: p<0.05	^{18}F-JK-PSMA-8: p<0.05 ^{18}F-DCFPyL: p<0.05
^{18}F-JK-PSMA-9	F(5,24)=5493 p<0.0001	F(1,24)=2121 p<0.0001	2 h: p<0.05 4 h: n.s.	2 h: p<0.05 4 h: p<0.05	^{18}F-JK-PSMA-9: p<0.05 ^{18}F-DCFPyL: p<0.05
^{18}F-JK-PSMA-11	F(5,24)=23040 p<0.0001	F(1,24)=10086 p<0.0001	2 h: p<0.05 4 h: p<0.05	2 h: p<0.05 4 h: p<0.05	^{18}F-JK-PSMA-11: p<0.05 ^{18}F-DCFPyL: p<0.05
^{18}F-JK-PSMA-12	F(5,24)=7254 p<0.0001	F(1,24)=2526 p<0.0001	2 h: p<0.05 4 h: p<0.05	2 h: p<0.05 4 h: p<0.05	^{18}F-JK-PSMA-12: p<0.05 ^{18}F-DCFPyL: p<0.05
^{18}F-JK-PSMA-14	F(5,24)=18304 p<0.0001	F(1,24)=4099 p<0.0001	2 h: p<0.05 4 h: p<0.05	2 h: p<0.05 4 h: p<0.05	^{18}F-JK-PSMA-14: p<0.05 ^{18}F-DCFPyL: p<0.05
^{68}Ga-PSMA-11	F(5,24)=848 p<0.0001	F(1,24)=287 p<0.0001	2 h: n.s. 4 h: n.s.	2 h: p<0.05 4 h: p<0.05	^{18}F-JK-PSMA-12: p<0.05 ^{18}F-DCFPyL: p<0.05

* Factor levels of "tracer/cell line/inhibitor" were:
- ^{18}F-DCFPyL, LNCaP C4-2 cells
- ^{18}F-DCFPyL + 2-PMPA, LNCaP C4-2 cells
- Tracer, LNCaP C4-2 cells
- Tracer + 2-PMPA, LNCaP C4-2 cells
- ^{18}F-DCFPyL, PC-3 cells
- Tracer, PC-3 cells

** Factor levels of "time" were:
- 2 h of incubation
- 4 h of incubation

"All others" were:
- ^{18}F-DCFPyL + 2-PMPA, LNCaP C4-2 cells
- Tracer + 2-PMPA, LNCaP C4-2 cells
- ^{18}F-DCFPyL, PC-3 cells
- Tracer, PC-3 cells

SUPPLEMENTAL TABLE 2: Statistical results of normalized cell uptake in LNCaP cells, 2-way ANOVA followed by Sidak's multiple comparison test.

Tracer	Uptake normalized to ^{18}F-DCFPyL after 2 h	Tracer vs. ^{18}F-DCFPyL*	2 h vs. 4 h**
^{18}F-DCFPyL	2 h: 100.0±1.7% 4 h: 202.7±4.2%	- -	p<0.05
^{18}F-JK-PSMA-7	2 h: 130.6±3.6% 4 h: 213.8±0.8%	2 h: p<0.05 4 h: p<0.05	p<0.05
^{18}F-JK-PSMA-8	2 h: 51.9±0.4% 4 h: 59.0±2.5%	2 h: p<0.05 4 h: p<0.05	n.s.
^{18}F-JK-PSMA-9	2 h: 76.4±1.9% 4 h: 194.3±7.1%	2 h: p<0.05 4 h: p<0.05	p<0.05
^{18}F-JK-PSMA-11	2 h: 71.5±1.6% 4 h: 203.2±1.0%	2 h: p<0.05 4 h: n.s.	p<0.05
^{18}F-JK-PSMA-12	2 h: 62.5±140.2% 4 h: 140.2±1.7%	2 h: p<0.05 4 h: p<0.05	p<0.05
^{18}F-JK-PSMA-14	2 h: 32.6±1.3% 4 h: 63.7±1.0%	2 h: p<0.05 4 h: p<0.05	p<0.05
^{68}Ga-PSMA-11	2 h: 104.7±5.8% 4 h: 205.1±7.1%	2 h: n.s. 4 h: n.s.	p<0.05

* Main effect of factor "tracer": $F(7,38)=1136$; $p<0.0001$

** Main effect of factor "time": $F(1,38)=6981$; $p<0.0001$

References

1. Drennen B, Scheenstra JA, Yap JL, et al. Structural re-engineering of the alpha-helix mimetic JY-1-106 into small molecules: disruption of the Mcl-1-Bak-BH3 protein-protein interaction with 2,6-di-substituted nicotinates. *ChemMedChem.* 2016;11:827–833.

2. Ehara T, Irie O, Kosaka T, et al. Structure-based design of substituted piperidines as a new class of highly efficacious oral direct Renin inhibitors. *ACS Med Chem Lett.* 2014;5:787–792.

3. Gajera JM, Gharat LA, Kattige VG, Khairatkar-Joshi N, Narayana L. Tricyclic compounds as mPGES-1 inhibitors. *Patent WO2012110860A1.* 2011.

4. Kim DW, Jeong HJ, Lim ST, Sohn MH. Tetrabutylammonium tetra(tert-butyl alcohol)-coordinated fluoride as a facile fluoride source. *Angew Chem Int Ed Engl.* 2008;47:8404–8406.

5. Murelli RP, Zhang AX, Michel J, Jorgensen WL, Spiegel DA. Chemical control over immune recognition: a class of antibody-recruiting small molecules that target prostate cancer. *J Am Chem Soc.* 2009;131:17090–17092.